

EFFECTS OF REDUCED GRAVITY ON NUCLEATE BOILING

BUBBLE DYNAMICS IN WATER

by R. Siegel and E. G. Keshock

Lewis Research Center
National Aeronautics and Space Administration
Cleveland, Ohio

E-2037

ABSTRACT

12315

A study was made of nucleate boiling bubble dynamics in distilled water under various reduced gravity fields. The nucleation occurred on a very smooth horizontal nickel surface at low heat fluxes. Since, because of the smooth surface finish, only a few nucleation sites were active, it was possible to photograph individual bubbles that were not interfered with by adjacent bubble columns. Data were taken at seven different gravity fields in the range from 1.4% to 100% of earth gravity by placing the apparatus on a counterweighted falling platform. Measurements were made of bubble departure diameters and frequencies, growth rates, contact angles, base circle diameters, and rise velocities. Comparisons were made to determine whether the measured gravity dependence of these quantities was in agreement with that predicted by correlations in the literature.

NOMENCLATURE

c_p specific heat at constant pressure

D bubble diameter

f bubble frequency

g gravitational field

k thermal conductivity

L latent heat of vaporization

q heat transferred per unit area from solid surface to liquid

FACILITY FORM 602

N 65-88642
(ACCESSION NUMBER)

(THRU)

(PAGES)

TMX-57461
(NASA CR OR TMX OR AD NUMBER)

(CODE)

(CATEGORY)

q_b heat transferred per unit area from vapor within a bubble to
bulk liquid

T temperature; T_w , surface temperature; T_{sat} , saturation temperature

ΔT temperature difference, $T_w - T_{sat}$

t time

u_∞ rise velocity of bubble far from boiling surface

α thermal diffusivity, $k/\rho c_p$

θ contact angle between bubble and surface

ρ density

σ surface tension

Subscripts:

d at detachment

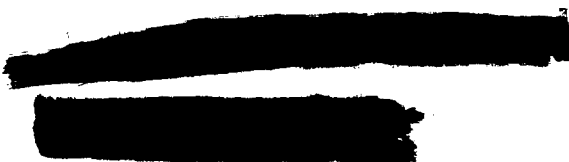
l liquid

n normal (earth) gravity

v vapor

INTRODUCTION

In the design of systems for space applications the effects of reduced gravity fields must often be considered. In an orbiting satellite or in space distant from planetary bodies, the gravity field will closely approach zero. In a system that is accelerating slightly, or on bodies such as the moon, the gravity field will be a fraction of that on earth. Heat-transfer processes such as pool boiling, condensation, and free convection are gravity dependent and hence would be expected to behave differently in reduced gravity fields. The effect of gravity has been indicated in numerous theoretical and experimental heat-transfer correlations by the presence



of a g factor. Although a number of experiments have been conducted to study high-gravity effects (1 to 4), there has been relatively little experimental work investigating the functional form of the g dependence in the reduced gravity range.

The present paper is concerned with bubble dynamics for saturated pool boiling in reduced gravity fields in the range from 1.4% to 100% of earth gravity. A previous paper (5), concerned mainly with burnout for low-gravity conditions, gives some information on rise velocities and bubble diameters at departure for boiling water. It was found that the departure diameters increased as $g^{-1/3.5}$ rather than $g^{-1/2}$, as is commonly indicated in correlations such as the Fritz equation. In the present study an improved apparatus was used, which permitted studies of bubble dynamics in greater detail. In (5), the nickel ribbon used as a test surface was generally quite crowded with nucleation sites, and bubbles probably interfered with each other. Consequently, the diameters measured at bubble departure were likely not those of single bubbles grown from a single nucleation site without interference from adjacent bubbles. Also, the nickel ribbon in (5) was only 0.2 inch wide, and hence the bubbles may have had a tendency to grow asymmetrically, that is, elongated in the direction along the ribbon length. This would be especially true under reduced gravity conditions where the bubbles can become quite large for boiling water.

In the present apparatus, boiling took place from a flat, horizontal circular area 7/8 inch in diameter. This permitted the bubbles to grow in all directions with equal ease. The test surface was carefully lapped and polished, which greatly reduced the bubble population in the low heat flux

range. This permitted the detailed observation of bubbles growing from a single site that were not interfered with by adjacent bubble columns, a condition not readily obtainable when using ordinary engineering surfaces. Since the theories of bubble growth generally deal with isolated bubbles, the intent was to obtain these idealized conditions experimentally in order to provide meaningful comparisons with isolated bubble theory. From the motion pictures of individual bubbles, measurements were made of departure diameters and frequencies, growth rates, dynamic contact angles, base circle diameters, and rise rates for six reduced gravity fields and for normal earth gravity.

The reduced gravity fields were obtained by placing the boiler and camera on a platform that could be raised and then dropped 12.5 feet. Different rates of downward acceleration were fixed by attaching counterweights of various sizes. When the counterweights were completely removed, there was still some friction in the system so that the lowest gravity field attainable was 1.4% of earth gravity.

Measurements in reduced gravity fields should be helpful for determining which theoretical predictions and experimental correlations are most general. For example, in (6) a correlation is briefly mentioned where the diameter of a departing bubble varies as $g^{-1/3}$ rather than $g^{-1/2}$ as in the Fritz equation, and differences of this type remain to be resolved. In departure theory a correction accounting for the bubble growth rate or the inertia associated with the bubble is generally neglected for normal gravity fields except in a few references such as (7) and (8). However, at low gravities the total buoyancy force on a bubble may become very small; hence,

the effect of inertia may become more significant. In the present study, the data will be compared with theories and correlations given in the literature to indicate which factors have increased importance when the gravity field is reduced.

EXPERIMENTAL APPARATUS

Counterweighted drop tower. - A simplified diagram of the drop tower is shown in Figure 1(a) and is a refinement of the apparatus used in (5) and (9). Part of the main structure of the tower was constructed by modifying a machine originally used to shock-test electronic equipment. The boiling experiment was mounted on an aluminum platform that could be dropped 12.5 feet before being decelerated by a sand bed. Vertical pipes mounted underneath the platform penetrated into the sand to bring the equipment to a gradual stop. The platform was centered between vertical rails by eight soft rubber wheels, which were in light contact with the rails and rotated freely on bearings. In order to obtain various fractional gravity fields, an adjustable counterweight was used to regulate the rate at which the platform descended. While the platform is being decelerated by the sand bed, the counterweights are decelerated by a friction brake mounted on the counterweight holder. No attempt was made to overcome all the friction in the system, which would be required for studying zero-gravity conditions. The minimum gravity attainable when the counterweight was removed was $0.014 g_n$.

Test boiler. - The boiler construction is illustrated in Figure 1(b). The boiling test surface is at the end of a copper rod, the base of which is heated by two 500-w. cartridge heaters. The circular boiling area is surrounded by a thin fin 0.020 in. thick, which is an integral part of the

rod. The entire piece was machined from a single large rod in order to prevent any boiling from cracks that might have developed at the junction between the rod and fin had they been two separate pieces. The fin attenuates the surface temperature so that boiling does not occur from the fin area or from the O-ring joint around the outside of the fin. This prevents bubbles from rising in the foreground, which would obscure photographing the test area.

The present study deals with individual bubbles originating from isolated nucleation sites. If several sites are present and closely spaced, the bubbles often interfere and sometimes merge with each other. This is especially true in low-gravity fields where the bubbles in water can grow quite large. Thus, it was desirable to have only a few widely separated sites on the surface. To limit the number of natural sites, the surface was carefully prepared. After machining, it was polished with fine emery cloth and then lapped to a $4\text{-}\mu$ in. rms roughness. Then it was given a thin nickel plating (about 0.0005 in.) and finally polished with a paste of water and very fine levigated alumina. The final polishing was repeated before each use of the boiler. With these surface conditions and a low heat flux, it was possible to obtain only one or two nucleating bubble columns on the $7/8$ -in.-diam. test area.

Two 250-w. cartridge heaters were mounted in copper fins extending through the top of the boiler. The fins provided a heat source along both sides of the liquid container that kept the fluid at the saturation temperature.

The boiler was mounted in a plywood box filled with powdered insulation. Only the test surface and glass enclosure were left exposed.

Instrumentation. - As shown in Figure 1(b), iron-constantan thermocouples were mounted in 0.030-in. holes at several positions along the axial length of the copper rod. Successive holes were spaced 90° apart around the periphery to provide as little interference as possible with the symmetry of the axial flow of heat. The thermocouple measurements gave the temperature gradient along the rod from which the heat flux could be evaluated. The temperature distribution was extrapolated to give the surface temperature. The temperatures were read by both a Brown recording potentiometer and a Rubicon precision potentiometer. The Brown recorder was useful because of its rapid indications of the temperature levels, which facilitated checking on the thermal equilibrium of the equipment.

Photographs were taken with a 16-mm Fastax high-speed motion picture camera. Lens extension tubes were used to magnify the field; generally an area about 1 by 3/4 in. was photographed. It was not desirable to use too great a magnification as the bubbles in low gravity can become so large that they grow out of the field of view. The camera speed was regulated with a Variac and was generally about 3500 frames per second. A 500-cycle square-wave generator (standard Fastax accessory) was used to place timing marks on the film every one-thousandth of a second.

Illumination was provided by a single 750-w. photo spotlight mounted about 5 in. above and 15 in. to the rear of the test surface. This type of backlighting was found to give good contrast so that the bubble outlines were clearly defined. A flat circular cell containing 1/2 in. of water between two pieces of plate glass was placed between the light and the boiler. This absorbed most of the heat from the light, and thus thermal equilibrium was not disturbed when the light was turned on.

The fluid temperature was measured with two thermocouples each mounted inside a stainless steel tube 0.0625 in. in diameter. One of the tubes was extended into the photographic field to provide a standard of size for calibrating the bubble measurements.

Before taking data, the rate of descent of the platform corresponding to various counterweight loadings was measured so that the effective gravity field on the platform would be known. All of these calibration runs were conducted under test conditions, that is, with all the necessary equipment mounted on the platform. Some small balancing weights were provided at each corner of the platform; these weights could be moved around to keep the platform balanced when the apparatus was rearranged without changing the total platform weight. A vertical measuring scale was fastened to the wall adjacent to the drop tower. For various counterweight sizes, the scale was photographed as the platform descended. The change of distance ΔS was read from the film for each time interval Δt as recorded by the timing marks on the film margin. A plot of $\Delta S/\Delta t$ as a function of t was then made, and the data gave a well-defined straight line for each counterweight size. The slope of this line was the platform acceleration, and earth gravity minus this acceleration gave the effective gravity field in which the boiling was taking place.

Experimental procedure. - The method of operation can be conveniently described by discussing a typical experimental run. The test surface was cleaned, polished, and wiped with tissue and distilled water, and the boiler was then assembled and filled with water. The upper heating fins were turned on to bring the water to the saturation temperature and drive off

dissolved gases. The test section was heated slowly in order to activate only a few nucleation sites. The water was boiled for a few hours to achieve a steady-state condition and for deaeration. If the number of active sites was excessive, this procedure was repeated until a situation was obtained where a steady stream of bubbles issued from only one or two sites.

With all instrumentation readied, the platform was raised into position and the counterweight loading was adjusted to provide the desired gravity field. The photographic light was turned on, and a switch was then closed which simultaneously started the camera and an Industrial timer. After a preset time interval (usually about $1/4$ sec.) the timer activated a solenoid release, which dropped the platform. As soon as the platform started to move, it energized a microswitch in the pulse generator circuit, which placed a light flash on the film margin to identify the beginning of the reduced gravity period. By providing a time delay before releasing the platform, the first part of each film recorded nucleation under normal gravity conditions so that comparisons could be made with the reduced gravity period immediately following. The counterweight was then adjusted to provide another gravity field, and the runs continued until the same nucleation site had been photographed in all the different gravity fields. Two or three 100-ft. rolls of film were taken for each site at each gravity field. Thermocouple readings were taken only with the platform at rest, as the thermal capacity of the system was too large for temperature changes to occur during drops of approximately 1-sec. duration.

RESULTS AND DISCUSSION

In this section the experimental results will be presented and compared with some of the theories given in the literature. First a discussion of the test conditions is warranted. The total duration of each test run was about 1 sec. The runs were initiated from a steady-state condition at normal gravity, and hence the heat flux and surface temperature are initially at an equilibrium condition corresponding to $1 g_n$. The duration of the reduced gravity period is sufficiently short so that, considering the high thermal capacity of the heating plate, the temperature distribution of the test surface probably does not change appreciably. Hence, during the test, the conditions are probably not identical to those for equilibrium at low gravity. However, in (5), measurements for nucleate boiling in reduced gravity indicated that the curve of q against $T_w - T_{sat}$ depends only slightly on gravity in the reduced gravity range. Hence, the present tests may be close to equilibrium as far as these quantities are concerned, but additional data are needed to confirm this. Another consideration is the temperature distribution in the fluid layer near the surface. For boiling in normal gravity there is a thin layer of superheated liquid near the surface. For low surface heat fluxes the thickness of this layer is partially governed by free convection, and hence it would be expected that the layer thickness would increase when gravity is reduced. The analysis in (10) can be used to provide a rough indication of the transient time required to establish a free-convection boundary layer. This indicates that if a heat-flux were suddenly applied to a plate in reduced gravity the transient time varies

as $1/(g/g_n)^{0.4}$ and hence can become large when g becomes very small. For the heat flux range in these studies ($q \sim 11,000-18,000$ B.t.u./hr.-ft.²) and $g/g_n = 0.1$, the transient time for a plate with a characteristic length of 1 in. is about 3 sec.. Hence, some transient effects may be present in the liquid at the lower gravities and should be kept in mind when evaluating the present work. It would be desirable to have longer periods of reduced gravity, but this is difficult because of the large height required for the counterweighted drop tower.

The boiling films were analyzed by viewing them on a Vanguard Motion Analyzer, which projected a magnified image on a ground glass screen. To obtain the best possible comparisons with theory based upon single isolated bubbles, measurements were made only on bubbles growing from single nucleation sites. In some instances, after a bubble was partially grown, other nucleation sites would be initiated near the bubble base, and this would cause small bubbles to merge with the original bubble. Measurements were not made for this type of bubble.

Nucleation cycle in reduced gravity. - As the gravity field is reduced, the bubbles begin to rise very slowly because of the decreased buoyancy force. This leads to a bubble coalescence mechanism that is much less frequently observed during normal gravity boiling. After a bubble departs and begins to move upward, if its rise velocity is small, the next bubble growing at the surface will collide with it because of the rapid rate at which the bubble diameter increases during the early stages of growth. When the gravity field is only a few percent of normal gravity, a bubble will detach and then remain close to the surface for perhaps 0.1 sec..

During this time the bubbles formed at the nucleation site will contact the detached bubble and merge with it, thereby being pulled from the surface before they can grow very large. This is shown by the sequence of photographs in figure 2(b). Several bubbles will rapidly feed into the larger bubble until it finally rises out of range. Then the next bubble will grow in an undisturbed manner.

The low-gravity boiling regime is thus characterized by a distinctive cyclical behavior. An undisturbed bubble will grow to its final size and detach in a normal manner. Then several small bubbles will pump into it before it can rise away from the surface. The large bubble thus serves as a temporary vapor sink near the surface and absorbs the new bubbles while they are relatively very small. The bubble frequency is quite high when the small bubbles are pumping into the larger one. This could greatly increase the turbulence induced near the surface, which would promote a high heat-transfer coefficient. Hence, this portion of the bubble cycle could play an important role in reduced gravity boiling heat transfer.

Another bubble coalescence mechanism, which may have some similarity to the present bubble cycle, is the hydrodynamic transition from isolated bubbles to continuous vapor columns discussed in (11). Hence, it is of interest to compare the present results with the formula derived in (11), which predicts when this transition should take place:

$$q_{\text{transition}} = 0.11 \rho_v I \theta^{1/2} \left(\frac{g \sigma_{lv}}{\rho_l - \rho_v} \right)^{1/4} \quad (1)$$

For site 2 the heat flux was 17,700 B.t.u./ (hr.) (sq. ft.) (see table I), and during most of the bubble growth period the contact angle was about 47° (table III (b)). For these conditions, equation (1) can be solved

for the gravity field at which transition should occur, and this gravity field is found to be about 1% g_n . However, coalescence was observed at higher gravities as evidenced in Figure 2(b) which depicts conditions for 6.1% g_n , and thus equation (1) does not agree with the present results. The discrepancy may result from using u_∞ as the bubble rise velocity near the surface in the derivation of equation (1). As discussed later, results of the present study indicate that the rise velocity immediately after bubble detachment is much smaller than u_∞ , which is not attained until the bubble has risen about 0.7 in. from the surface. Using a lower velocity than u_∞ would increase the predicted gravity field at which transition should occur for a given q and bring equation (1) into better agreement with the present observations.

Diameter of bubbles at departure. - The diameters of single bubbles were measured at the instant that they broke away from the surface. In many instances the bubble formed a short cylindrical neck joining it to the surface, and this short vapor column was pinched off (generally not right at the surface) at the instant of departure (see Figure 2(a)). Thus, a small vapor mass was left behind which served as a nucleus for the next bubble. The height and width of the bubble were measured at departure, and the average of these measurements was used as the diameter. In the beginning portion of each film roll, there were generally about 10 bubbles in the normal gravity period that were not interfered with. For each film roll, an arithmetic average diameter was computed for these bubbles and is given in the columns labeled N (normal gravity) in table II(a) for four different nucleation sites. For each site the values in the N

columns were averaged to give a final average for the normal gravity condition, and these values are listed in the column labeled $D_{d,n}$.

As the gravity fields were progressively reduced, the bubbles became much larger and had considerably longer growth times. At several percent of normal gravity only two or three bubble histories could be photographed on a roll of film, while for $0.429 g_n$ there were about 20 bubble histories. Hence, the average values given in the columns labeled R (reduced gravity) in table II(a) have a greater statistical weight for the higher gravities. For $0.014 g_n$ the growth time was approximately equal to the length of the test run; hence, only a small amount of data is given because of the difficulty of obtaining a complete history for a bubble that had not been interfered with during its growth.

The variation of bubble diameters is given in Figure 3 as a function of the fraction of normal gravity g/g_n . Each data point corresponds to the average departure diameter at a particular site and reduced gravity, divided by the average of all the normal gravity data taken at that site. The solid line is drawn through the average of the data points at each gravity with the exception of the point at $g/g_n = 0.014$.

Several theoretical relations have been proposed for predicting the size of bubbles at departure from a horizontal surface, and some of these will now be considered. The best known is the Fritz (12) equation,

$$D_d = 0.0208 \theta \left[\frac{\sigma_{lv}}{g(\rho_l - \rho_v)} \right]^{1/2} \quad (2)$$

where the contact angle θ is in degrees.

A relation by Zuber (6) is

$$D_d = \left[\frac{6\sigma_{LV}}{g(\rho_L - \rho_V)} \frac{k \Delta T}{q} \right]^{1/3} \quad (3)$$

A correlation given by Staniszewski (8) is

$$D_d = 0.0071 \theta \sqrt{\frac{2\sigma_{LV}}{g(\rho_L - \rho_V)}} \left[1 + 0.435 \left(\frac{dD}{dt} \right)_d \right] \quad (4)$$

where dD/dt is in inches per second.

Cole (13) gives the equation

$$D_d = 0.040 \theta \left[\frac{\sigma_{LV}}{g(\rho_L - \rho_V)} \right]^{1/2} \left[\frac{g\sigma_{LV}}{u_d^4(\rho_L - \rho_V)} \right]^{-0.22} \quad (5)$$

First consider how well these equations predict the departure diameters for normal gravity. The data for sites 1 and 2 are given as follows:

Site	Experimental			Computed		
	$D_{d,n}$ in.	θ , deg.	$(dT/dt)_{d,n}$ in./sec	$D_{d,n}$, in.		
				Eq. (2)	Eq. (3)	Eq. (4)
1	0.093	38	1.0	0.078	0.065	0.054
2	.134	47	1.0	.096	.064	.067

The q and ΔT needed for Equation (3) are given in table I. The values of $(dD/dt)_d$ for Equation (4) have been taken from Figures 5(a) and (b) and are approximate average values. All of the predicted diameters are too low and the best results are given by Equation (2), although the values are still about 20% too low. No results were computed from Equation (5) because it was not possible to determine accurately the magnitude of u_d , the bubble

rise velocity at departure. This is especially true as gravity is reduced because the rise velocity immediately after departure is very small. This is evident from the bubble paths given in Figure 8(a), which indicate the difficulty of defining the slope of the curve at departure.

Since the departure diameters for normal gravity have been discussed at great length in the literature, we turn after this brief discussion to the gravity dependence aspects. Equation (2) contains both a gravity factor and the contact angle at departure. The data in table III indicate that for a particular nucleation site the contact angle does not depend significantly on g . Hence, Equation (2) predicts $D_d \sim g^{-1/2}$, which is the trend of the data in Figure 3 for g/g_n less than about 0.1. For $g/g_n > 0.1$ the trend is more like $g/g_n^{-1/3}$, as indicated by Equation (3). Equation (4) has a dynamic growth factor $(dD/dt)_d$, which depends on g . Values of $(dD/dt)_d$ obtained from Figures 5(a) and (c) for site 1 are as follows:

g/g_n	$(dD/dt)_d$, in./sec.	$D_d/D_{d,n}$
1.0	1.0	1.0
.429	.8	1.43
.229	.4	1.71
.126	.5	2.38
.061	.2	3.06
.030	.2	4.38
.014	.3	6.65

These values are only approximate because of the difficulty in measuring the slopes of the growth curves obtained from the data. With θ independent of g , Equation (4) gives

$$\frac{D_d}{D_{d,n}} = \left(\frac{g}{g_n} \right)^{-1/2} \left[\frac{1 + 0.435(dD/dt)_d}{1 + 0.435(dD/dt)_{d,n}} \right] \quad (4a)$$

Calculated values for $D_d/D_{d,n}$ are listed in the previous table. The dynamic growth factor in brackets in Equation (4a) brings the theory into better agreement with the experimental data as shown in Figure 3. In the low-gravity range the values of $(dD/dt)_d$ become small and fairly constant, and hence Equation (4a) reduces to almost a $(g/g_n)^{-1/2}$ variation, which agrees with the trend of the data. From this it appears that the dynamics of bubble growth have significant effects on the departure diameter.

Frequency of single undisturbed bubbles. - It is first necessary to clearly define the frequency discussed here. For the nucleation sites that were observed, the waiting time between the departure of a bubble and the beginning of the next bubble was always zero and consequently does not have to be accounted for in the present calculations. Hence, the frequency is defined here as the reciprocal of the growth time for single undisturbed bubbles. It is thus an idealized frequency that would exist if the site were emitting a stream of bubbles, none of which ever coalesced with each other. Actually, as described previously, there are periods of very high bubble frequency not considered here, where bubbles are being formed and removed from the surface by a large bubble that remains close to the surface because of its low rise rate in reduced gravity.

Table II(b) presents the average frequency at each site for both the reduced gravity and normal gravity portions of each film roll. The column labeled f_n gives the average for each site of all the normal gravity frequencies. The ratio f/f_n has been plotted in Figure 4(a), which shows

a general trend of f decreasing directly with g . This means the bubble growth times become much larger when gravity is reduced. However, this may not always be the case as evidenced by the data from site 2, where f/f_n is practically constant in the reduced gravity range. These data have a higher q and Δt than the other three sites, but definite conclusions as to the influence of q and Δt cannot be made without additional data at higher heat fluxes.

Figure 4(b) presents the gravity dependence of the frequency-diameter product. A general gravity dependence is indicated that is on the order of $fD \sim g^{1/2}$. For each nucleation site, however, fD appears to have a tendency to become constant as g is reduced.

In (14) a correlation is presented where $fD^{1/2}$ was found to vary as $g^{1/2}$. The present data have been so correlated and are shown in Figure 4(c). The data are quite scattered and do not follow the predicted trend. As in Figure 4(b) there is a tendency for the curves at each site to become less dependent on g as g is reduced. The leveling out appears to be a function of the heat flux (or ΔT) and implies that the frequency-diameter product becomes less dependent on gravity as the heat flux is increased.

Bubble growth rates. - When investigating the boiling process by examining the details of bubble dynamics, a factor of fundamental importance is the rate of growth of bubbles while they are attached to the surface. In the present experiments the water was always at the saturation temperature so that growth and collapse in subcooled liquids were not considered. There are several experiments in the literature on growth rates under normal gravity conditions, and there are considerable mathematical analyses

providing growth rate predictions. Since the present work is primarily concerned with the effect of gravity, these references will not be reviewed in detail. The experimental results will be compared with a few of the predictions, and additional information on previous growth rate work can be found, for example, in (15) and (16). The growth rate predictions have not indicated a gravity dependence (gravity of course has an effect upon the departure time), and one of the objects of the present study is to determine whether or not a gravity dependence is physically exhibited.

The growth rate predictions used for comparison will now be listed. Fritz and Ende (17) considered bubble growth in an infinite uniformly superheated liquid. The heat conduction into the bubble was determined by having the temperature profile in the liquid adjacent to the bubble boundary equal to that for unsteady heat conduction in a slab. Their analysis resulted in the equation

$$D = \frac{4k \Delta T}{L\rho_v \sqrt{\pi\alpha}} t^{1/2} \quad (6)$$

Flesset and Zwick (18) included the influence of liquid inertia and accounted for the effect of the spherical shape of the boundary upon the temperature profile, rather than using the temperature distribution in a slab as done by Fritz and Ende. This gave the result

$$D = \sqrt{3} \frac{4k \Delta T}{L\rho_v \sqrt{\pi\alpha}} t^{1/2} \quad (7)$$

which is the same as Equation (6) except for a $\sqrt{3}$ factor.

Forster and Zuber (19) derived a similar expression

$$D = \frac{\pi}{2} \frac{4k \Delta T}{L \rho_v \sqrt{\pi \alpha}} t^{1/2} \quad (8)$$

which is again the same as the previous expressions except the constant in front is now $\pi/2$. Zuber (20) considered growth in a nonuniform temperature field and introduced a correction factor for sphericity to obtain

$$D = \frac{\pi}{2} \left[\frac{4k \Delta T}{L \rho_v (\pi \alpha)^{1/2}} t^{1/2} - \frac{2q_b}{L \rho_v} t \right] \quad (9)$$

All of these expressions were derived for growth in an infinite medium away from solid surfaces. Surface tension, viscosity and inertia were not considered to be important. Equations (6), (7), and (8) indicate a steady increase of diameter with the square root of time, while Equation (9) predicts that a maximum diameter will be reached. More elaborate growth models have been given, for example, in (7), which includes inertia and surface tension for a bubble growing on a surface. The equations must be evaluated numerically, and, since this was not carried out in (7), it is not known whether the model would provide improved results.

First the growth rate curves will be examined for normal gravity. These are shown in Figures 5(a) and (b) for sites 1 and 2. For clarity only a few representative curves have been shown, although all other data fell within these ranges. The growth rates for the two sites differ somewhat because the test conditions are not the same as shown in table I. For comparison with theory the bubbles selected for measurements were of

symmetrical shape and were interfered with as little as possible by preceding bubbles.

For both sites the Plesset-Zwick and Forster-Zuber predictions are too high. For site 1 both the Fritz-Ende and Zuber predictions provide reasonable agreement with the data. For site 2, Zuber's curve lies closest to the experimental points. However, as will be shown later, Equation (9) does not seem physically realistic because it predicts that a maximum bubble size will be reached, and this is not found experimentally.

Considering now the reduced gravity range, growth curves for site 1 have been plotted on Figures 5(c) and (d). Additional data are given in table III(b) for site 2. The data for gravity fields equal to and above $0.061 g_n$ are for bubbles that were typical of several bubbles that were examined at each reduced gravity. For 0.014 and $0.03 g_n$ the growth times were very long and so it was difficult to obtain a complete bubble cycle during the test time available. Hence, the data plotted for these fields represent only a single bubble. Whether or not the bubbles measured were typical is uncertain in view of the lack of additional bubbles to compare with. Thus, the very low gravity data should be given less statistical weight.

In the logarithmic plot (Figure 5(d)) the Fritz-Ende relation offers the best general agreement over the entire range of data. However, if the data are grouped into initial (< 0.02 sec.) and final (> 0.02 sec.) growth periods, this relation does not indicate the observed diameter variation during the final growth period. The data indicate $D \sim t^{3/8}$ compared with $t^{1/2}$ from theory. In the initial growth period the time

exponents were observed to range from 0.5 to 0.8. Staniszewski (8) observed that generally the exponent is greater than $1/2$ and sometimes reaches the value of 1 in the early stage of bubble growth; afterwards it decreases with time and in the late stage is approximately $1/3$. The total growth time in his experiments was on the order of only 0.030 sec., however, which is characteristic of normal gravity. For all the bubbles observed in the present study the same qualitative behavior was indicated by the data. Usually the decrease in growth rate occurred about 0.010 to 0.020 sec. after initiation of the bubble.

It is interesting to note that for even the longest bubble cycles (0.76 sec.) a maximum bubble size was not attained. In observations of normal gravity bubble growth rates, the combination of short cycle times and scatter in measurements could give the impression that a maximum bubble size will be reached (when $dD/dt = 0$), which indicates a deficiency of energy available to maintain a net vapor formation. However, the very long growth times that occur in low-gravity fields do not give evidence of such a deficiency. This is indicated in Figure 5(d), where bubbles are observed to grow steadily in accordance with the relation $D \sim t^n$. In Equation (9) the correction term $-2q_b t / L\rho_v$ causes the bubble to reach a maximum diameter, whereas a maximum is not indicated by the data. In order for the theoretical curve to agree with the data it would be necessary for the maximum in the theoretical curve to occur at a time after the observed bubble detachment. Possibly the quantity q_b should be less than the heat flux q , as assumed in (20), and should also be a function of gravity. The growth analysis in (16) is of interest in that it offers a

possibility for including a gravity dependence having a physical basis. The theory depends on the thickness of a thermal layer of heated fluid adjacent to the surface. In the region of low heat flux the thermal layer thickness may partly depend on free convection, and, hence, the layer thickness would be a function of g . This will be investigated in the future after additional data have been obtained for water and other fluids.

Dynamic contact angles. - A parameter that may influence bubble departure diameters and growth rates is the time variation of contact angle (dynamic contact angle) between the bubble and the surface while the bubble is growing. In the present investigation, contact angle measurements were made during bubble growth for six reduced gravity fields in addition to normal earth gravity. For each data point the contact-angle was measured at both sides of the bubble and averaged arithmetically. It was found very difficult to make accurate contact angle measurements because extreme clarity and high magnification are required before one can tell whether the actual contact angle at the root of the bubble is being measured rather than the slope of the bubble close to the root. In view of the considerable judgment and interpretation required for these measurements, the accuracy is estimated to be within about 10° . However, since one person reads a given set of data with the same interpretation throughout, the accuracy of readings relative to one another is better.

Contact angle measurements are shown in Figure 6 for bubbles growing at site 1 in three different reduced gravity fields. Data for other gravity fields have been omitted for clarity but are tabulated in tables III(a) and (b). Generally for each bubble the contact angle was

found to remain approximately constant during growth, except for short time intervals at the beginning and end of the growth period. In addition, for site 1 (table III(a)) the contact angle did not vary appreciably with the magnitude of the reduced gravity field. For site 2 (table III(b)) the contact angle decreased slightly as gravity was reduced. It was observed that, when a bubble begins to detach, a short cylindrical neck is often formed between the bubble and the surface. During this formation the contact angle increases toward 90° . This is not shown in Figure 6 because the curvature of a bubble at the surface is often so abrupt that the slope may not be measured accurately.

Han and Griffith (7) propose a criterion for departure diameters that is dependent upon the dynamic contact angle. In their experiments the departure size was found to be a function of the "receding dynamic contact angle" rather than an average contact angle, which is normally used. In their examination of Staniszewski's experiments (8), which indicated a dependence of departure size upon bubble growth rate, they suggest that these apparent dynamic effects upon departure size should instead be attributed to changes in contact angle. In view of the constancy of the contact angle for the very long growth times examined herein, it seems more reasonable that contact angle changes are not a cause for departure of the bubble, but instead are a consequence of the distortion caused by its impending departure.

Bubble base width. - The width of the bubble base at the surface (contact circle diameter) was measured during bubble growth at two sites for seven gravity fields. The data are given in tables III(a) and (b),

and some of the data has been plotted in Figure 7, which gives the base width during growth at site 1 for four reduced gravities. All of the curves have a rapid initial increase in base width. The width may not actually start from zero in all cases because sometimes there is a small vapor mass left behind when the previous bubble detaches. Throughout most of the growth period the base width remained reasonably constant and then decreased rapidly as the bubble began to detach. Since detachment often resulted from the breaking of a short cylindrical neck between the bubble and surface, the base at the surface does not necessarily drop to zero.

Figure 7 shows that for bubbles from site 1 the maximum base width achieved during growth increases notably with decreasing gravity. For site 2, however, as may be seen from table III(b), the increase is much less. As shown in table I, the heat flux for site 2 was larger than that for site 1 so that the gravity dependence may be a function of this parameter.

In (16) (see Figure 11 of that reference) the relation between the bubble base width and the bubble height is discussed with respect to the computations in (21). For bubbles up to a range of about 1/16 inch in diameter the results in (21) predict bubble base radii approximately equal to bubble height. The present base sizes are considerably smaller, as illustrated by the normal gravity bubble in Figure 2(a).

Rise velocity of detached bubbles. - The data for site 1 were taken at a little lower magnification than for the other sites. Thus, the pictures covered sufficient area so that bubbles could be followed for about 1 in. of rise from the surface. Bubbles were selected that appeared to have as little interference as possible from other bubbles in the column.

For normal gravity, measurements were made for several bubbles, and a typical bubble path is shown in Figure 8(a), which gives the height of the center of gravity above the surface as a function of time. After the bubble has moved upward about 0.7 in., the slope of each curve becomes constant and gives the freely rising velocities listed in table IV. The velocities for normal gravity were in the range between 11.3 and 12.1 in./sec. An equation from (22),

$$u_{\infty} = 1.18 \left[\frac{\sigma_L g (\rho_L - \rho_V)}{\rho_L^2} \right]^{1/4} \quad (10)$$

predicts a u_{∞} of 7.26 in./sec. for normal gravity, which is substantially less than the measured values. According to (23) the constant in Equation (10) should be 1.53, which would give better agreement. Some bubble paths for reduced gravity are illustrated in Figure 8(a). The vertical line drawn through some of the curves gives the time after which no more bubbles generated at the surface coalesce with the rising bubble. For 0.014 g_n the coalescence process had not been completed when the run ended. Velocities computed from the slope at the upper ends of the curves are given in table IV. Figure 8(b) gives the ratio $u_{\infty}/u_{\infty,n}$ as a function of gravity. Equation (10) indicates that $u_{\infty}/u_{\infty,n} \sim (g/g_n)^{1/4}$, and this is in very good agreement with the data shown in Figure 8(b) except at the lowest gravity. For this gravity, it was not possible to follow the bubble very far before the low-gravity period ended because of its slow rate of rise. Hence, the bubble had not accelerated to its final steady velocity.

CONCLUDING REMARKS

One of the most notable observations on the effects of reduced gravity on bubble dynamics was the very rapid removal of small vapor bubbles from the boiling surface by a previously detached bubble that momentarily remained just above the surface because of its slow rise rate. The nucleation in low gravity cannot be thought of as a succession of large bubbles at low frequency, but rather as one large bubble, then several small bubbles of high frequency that are absorbed by the large bubble, and then a large bubble again. The large bubbles thus serve as temporary reservoirs for removing vapor from the surface. The average bubble frequency is actually much higher than that for the particular bubbles measured here, which are those not interfered with. This helps maintain a high turbulence level near the surface so that as the gravity field is reduced the heat-transfer coefficients may still remain high.

It was not possible to measure heat-transfer coefficients with the present apparatus because of the short duration of the tests and the large thermal capacity of the heating surface. It is planned to make these measurements in the future by using a very thin wire as a heating element. This type of heating element is not desirable for studies of bubble dynamics, however, because the surface area is so small. This is especially true in reduced gravity where the bubbles become quite large for boiling water.

For the single bubbles measured herein, it was found that the diameters at departure increased approximately as $g^{-1/3}$ for fields between 0.1 and $1 g_n$, and for lower gravities increased as $g^{-1/2}$. The latter is the functional relation predicted from considering a balance of surface tension

and buoyancy forces at departure. The inclusion of a dynamic term, dD/dt , as suggested by Staniszewski (8) gave an improved correlation, so it appears likely that dynamic forces do play a significant role in bubble departure.

The results for the frequency-diameter product at departure were much more scattered than the departure diameters. There was a general trend of fD to decrease as gravity was reduced and then tend to become fairly constant below a certain gravity. The gravity at which the curve became more nearly constant increased with q so that for higher q 's it is possible that fD may become independent of gravity.

In reduced gravity the bubbles become quite large, and the growth times are long compared with those in earth gravity. The bubble size increases continuously, according to the approximate relation $D \sim t^n$ where $n = 0.5$ to 0.8 for $t < 0.02$ sec. and $n \approx 3/8$ for $t > 0.02$ sec.. The growth curves can be approximated fairly well by a $t^{1/2}$ behavior, but this does not reveal that the growth rate is actually much more rapid during the initial stages than during the final stages. Even after long growth periods the bubbles do not exhibit a tendency to reach a constant diameter as has been postulated in one of the growth theories.

The bubble contact angle was found to be essentially independent of gravity. Also, during the relatively long growth periods for reduced gravity, the contact angle remained substantially constant except during a short initial period and near bubble departure. The larger bubbles in reduced gravity were accompanied by larger base widths (contact circle diameters).

The rise velocity of bubbles after departure is initially small and then increases to a steady value after the bubble has moved about 0.7 in. from the surface. This steady value is a function of gravity and was found to agree very well with theory predicting $u_{\infty} \sim gl^{1/4}$.

The preceding results are all for individual bubbles formed on a flat horizontal surface in distilled water. For a more viscous liquid the drag and dynamic forces may have a different relation to the buoyancy force, and hence the behavior in reduced gravity could be considerably different than the present results. Some preliminary studies have exhibited this and will be the subject of future study.

REFERENCES

1. H. Merte, Jr., and J. A. Clark, "Pool Boiling in an Accelerating System," (Trans. ASME), Jour. Heat Transfer, vol. 83, no. 3, Aug. 1961, pp. 233-242.
2. C. P. Costello, and W. E. Tuthill, "Effects of Acceleration on Nucleate Pool Boiling," Paper Presented at AIChE-IMI Meeting, Mexico City, June 1960.
3. R. W. Graham, and R. C. Hendricks, "A Study of the Effect of Multi-G Acceleration on Nucleate-Boiling Ebullition," NASA TN D-1196, 1963.
4. H. J. Ivey, "Acceleration and the Critical Heat Flux in Pool Boiling Heat Transfer," (To be publ. by Inst. Mech. Eng.).
5. C. M. Usiskin, and R. Siegel, "An Experimental Study of Boiling in Reduced and Zero Gravity Fields," (Trans. ASME), Jour. Heat Transfer, vol. 83, no. 3, Aug. 1961, pp. 243-253.
6. N. Zuber, "Hydrodynamic Aspects of Boiling Heat Transfer," Ph.D. Thesis, Univ. Calif., June 1959.
7. Chi-Yeh Han, and P. Griffith, "The Mechanism of Heat Transfer in Nucleate Pool Boiling," Rep. 7673-19, Dept. Mech. Eng., M.I.T., Mar. 1962.
8. B. E. Staniszewski, "Nucleate Boiling Bubble Growth and Departure," Tech. Rep. 16, Div. Sponsored Res., M.I.T., Aug. 1959.
9. R. Siegel, and C. M. Usiskin, "A Photographic Study of Boiling in the Absence of Gravity," (Trans. ASME), Jour. Heat Transfer, vol. 81, no. 3, Aug. 1959, pp. 230-236.

E-2037

10. R. Siegel, "Transient Free Convection from a Vertical Flat Plate," ASME Trans., vol. 80, Feb. 1958, pp. 347-359.
11. R. Moissis, and P. J. Berenson, "On the Hydrodynamic Transitions in Nucleate Boiling," Paper 62-HT-8, ASME, Aug. 1962.
12. W. Fritz, "Calculation of the Maximum Volumes of Vapor Bubbles," Phys. Zeit., vol. 36, 1935, p. 379.
13. R. Cole, "A Photographic Study of Pool Boiling in the Region of the Critical Heat Flux," AIChE Jour., vol. 6, Dec. 1960.
14. P. W. McFadden, and P. Grassmann, "The Relation Between Bubble Frequency and Diameter During Nucleate Pool Boiling," Int. Jour. Heat and Mass Transfer, vol. 5, Mar.-Apr. 1962, pp. 169-173.
15. P. H. Streng, A. Orell, and J. W. Westwater, "Microscopic Study of Bubble Growth During Nucleate Boiling," AIChE Jour., Dec. 1961, pp. 578-583.
16. Y. Y. Hsu, and R. W. Graham, "An Analytical and Experimental Study of the Thermal Boundary Layer and Ebullition Cycle in Nucleate Boiling," NASA TN D-594, 1961.
17. W. Fritz, and W. Ende, "Verdampfungsvorgang nach Kinematographischen Aufnahmen an Dampfblasen," Phys. Zeit., bd. 37, 1936.
18. M. Plesset, and J. A. Zwick, "The Growth of Vapor Bubbles in Superheated Liquids," Jour. Appl. Phys., vol. 25, 1954, p. 493.
19. H. K. Forster, and N. Zuber, "Growth of a Vapor Bubble in a Superheated Liquid," Jour. Appl. Phys., vol. 25, 1954, p. 474.
20. N. Zuber, "The Dynamics of Vapor Bubbles in Nonuniform Temperature Fields," Int. Jour. Heat and Mass Trans., vol. 2, Mar. 1961, pp. 83-98.

21. F. Bashforth, and J. C. Adams, "An Attempt to Test Theories of Capillary Action by Comparing the Theoretical and Measured Forms of Drops of Fluid," Cambridge Univ. Press, 1883, p. 80.
22. F. N. Peebles, and H. J. Garber, "Studies on the Motion of Gas Bubbles in Liquids," Chem. Eng. Prog., vol. 49, 1953, p. 88.
23. T. Harmathy, "Velocity of Large Drops and Bubbles in Media of Infinite or Restricted Extent," AIChE Jour., vol. 6, 1961, p. 281.

TABLE I. - HEAT FLUXES AND
TEMPERATURE DIFFERENCES
DURING DIFFERENT
TEST RUNS

Site	$q,$ $\frac{\text{B.t.u.}}{(\text{hr.})(\text{sq. ft.})}$	$T_w - T_{\text{sat}},$ $^{\circ}\text{F}$
1	10,900	11.1
2	17,700	17.0
3	12,700	12.4
4	12,700	12.4

E-2037

TABLE II. - BUBBLE DEPARTURE DIAMETERS AND FREQUENCIES AS A FUNCTION OF GRAVITY

(a) Departure diameter, in.

Gravity for test run, percent of g_n	100	42.9		22.9		12.6		6.1		3.0		1.4	
Site	$D_{d,n}$	N*	R*	N	R	N	R	N	R	N	R	N	R
1	0.093	0.088	0.117	0.094	0.146	0.092	0.181	0.093	0.257	0.089	0.363	0.098	0.479
2	.134	----	----	.134	.195	.135	.252	.134	.310	----	----	----	----
3	.106	.105	.139	.102	.176	.112	.222	.108	.380	.102	.484	----	----
4	.101	.078	.120	.104	.151	.106	.205	.109	.254	.106	.375	----	----

(b) Frequency, 1/sec.

Site	f_n	N	R	N	R	N	R	N	R	N	R	N	R
1	49.9	55.8	27.2	49.1	14.6	48.8	9.89	38.6	3.03	45.6	1.61	61.6	1.35
2	24.1	----	----	25.2	6.72	24.2	6.21	22.9	5.10	----	----	----	----
3	27.6	21.4	16.6	22.1	7.77	47.2	6.61	27.7	1.96	19.5	1.67	----	----
4	59.0	58.3	36.5	58.4	23.8	54.7	6.80	61.3	4.84	62.3	2.47	----	----

*N and R refer to normal and reduced gravity portions of a test run.

TABLE III. - VARIATION WITH TIME OF AVERAGE DIAMETER, CONTACT ANGLE, AND BASE WIDTH, AS A FUNCTION OF GRAVITY

(a) Site 1.

100% Gravity ^a				42.9% Gravity				22.9% Gravity				12.6% Gravity			
Time, msec.	Av. diam., in.	Contact angle, deg.	Base width, in.	Time, msec.	Av. diam., in.	Contact angle, deg.	Base width, in.	Time, msec.	Av. diam., in.	Contact angle, deg.	Base width, in.	Time, msec.	Av. diam., in.	Contact angle, deg.	Base width, in.
1	0.014	--	----	1	0.021	--	----	1	0.010	--	----	1	0.012	--	----
3	.032	37	0.010	3	.037	37	0.014	3	.023	--	----	7	.038	34	0.011
5	.048	38	.014	5	.049	37	.015	5	.038	45	0.012	11	.048	34	.016
7	.059	36	.014	7	.059	39	.016	7	.051	45	.015	16	.064	34	.017
10	.073	37	.015	10	.072	38	.015	11	.077	42	.025	26	.086	34	.019
12	.077	38	.014	12	.075	38	.017	16	.094	38	.019	43	.109	32	.026
15	.083	38	.019	15	.080	38	.024	21	.106	34	.017	57	.128	31	.032
18	.086	39	.017	20	.088	38	.021	31	.119	34	.013	76	.149	35	.034
20	.088	40	.016	25	.097	39	.019	51	.136	37	.013	88	.156	34	.034
22	.090	42	.014	30	.101	--	.010	61	.141	38	.012	100	.164	33	.032
25	.095	--	.013	36	.107	--	.003	70	.144	--	----	114	.174	34	.038
6.1% Gravity				3.0% Gravity				1.4% Gravity							
1	0.009	--	----	1	0.011	--	----	1	0.024	--	----				
2	.024	--	----	2	.024	33	0.004	3	.044	38	0.016				
4	.036	36	0.014	5	.047	34	.016	13	.093	36	.033				
7	.054	37	.019	10	.080	38	.031	28	.131	38	.048				
10	.071	40	.028	16	.096	37	.026	51	.160	39	.058				
21	.109	34	.027	21	.112	38	.044	97	.204	38	.079				
51	.146	38	.058	45	.136	36	----	147	.236	36	.087				
97	.178	37	.058	85	.168	36	.059	207	.275	38	.088				
143	.200	37	.057	125	.194	35	.061	302	.318	32	.100				
188	.217	36	.060	175	.228	34	.062	387	.350	32	.102				
246	.236	36	.059	275	.272	32	.065	487	.378	33	.104				
298	.251	36	.056	425	.317	34	.062	607	.414	34	.112				
351	.263	34	.042	525	.339	36	.061	707	.440	34	.116				
368	.269	--	.012	623	.359	--	.014	757	.467	40	.064				

TABLE III. - Concluded. VARIATION WITH TIME OF AVERAGE DIAMETER, CONTACT ANGLE, AND BASE WIDTH,
AS A FUNCTION OF GRAVITY

(b) Site 2.

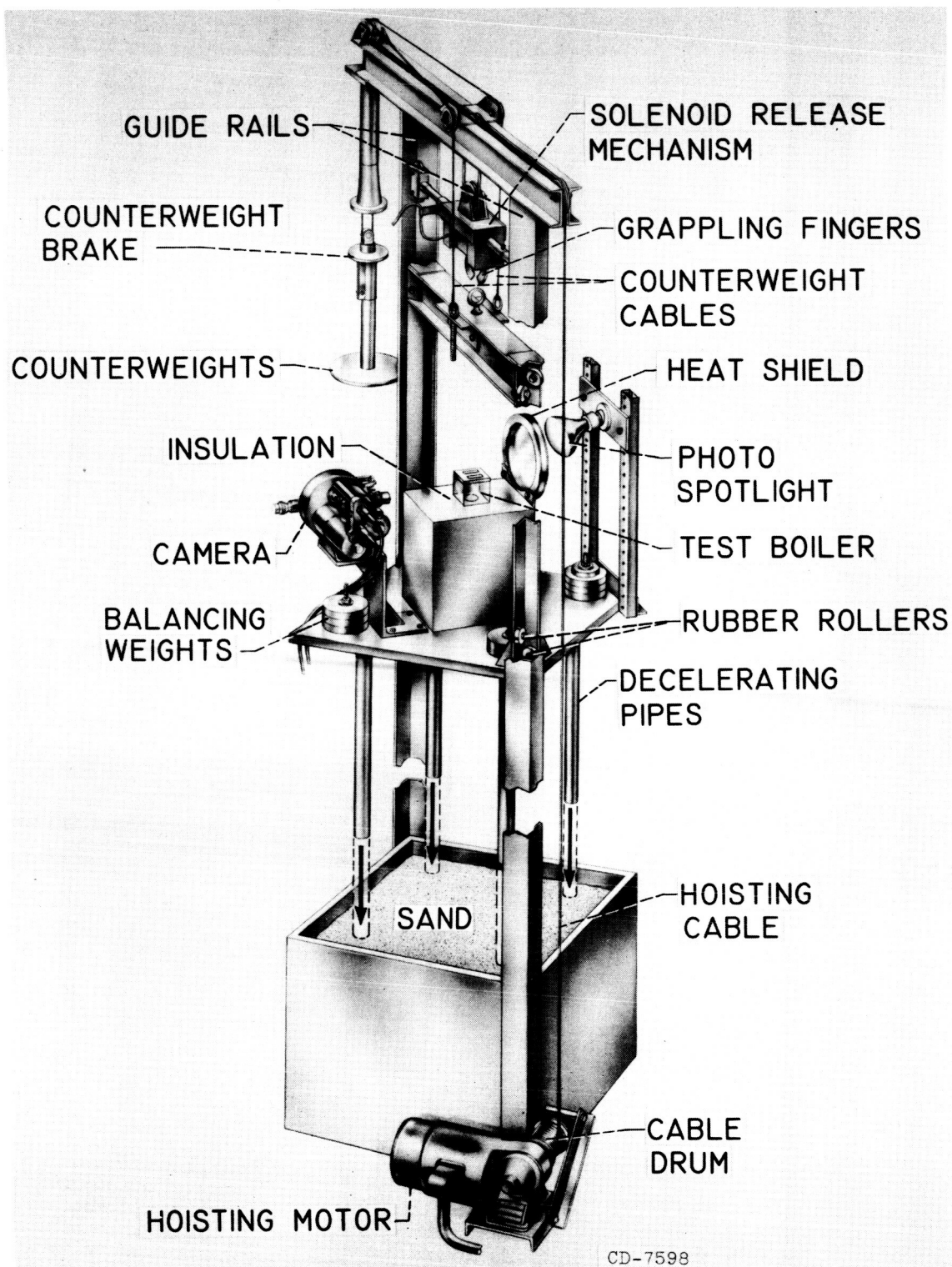
100% Gravity ^b				22.9% Gravity				12.6% Gravity				6.1% Gravity			
Time, msec.	Av. diam., in.	Contact angle, deg.	Base width, in.	Time, msec.	Av. diam., in.	Contact angle, deg.	Base width, in.	Time, msec.	Av. diam., in.	Contact angle, deg.	Base width, in.	Time, msec.	Av. diam., in.	Contact angle, deg.	Base width, in.
1	0.015	--	---	1	0.021	--	---	1	0.026	--	---	1	0.021	--	---
2	.024	--	---	3	.037	44	0.027	2	.034	--	---	2	.036	46	0.028
4	.040	44	0.025	5	.049	48	.030	5	.053	40	0.028	5	.056	46	.032
7	.059	46	.028	8	.065	46	.032	11	.076	44	.033	10	.076	46	.033
10	.073	43	.031	16	.087	43	.033	21	.114	43	.032	20	.113	45	.040
14	.087	45	.026	26	.108	42	.032	33	.133	37	.033	50	.190	35	.040
21	.101	46	.027	51	.137	36	.037	47	.154	38	.037	75	.224	35	.036
31	.119	50	.027	76	.160	42	.031	91	.197	39	.031	100	.253	34	.038
36	.128	58	.028	101	.171	40	.032	128	.221	46	.030	150	.293	43	.035
41	.130	72	.027	126	.184	42	.031	153	.241	50	.024	175	.303	81	.024
43	.128	--	---	154	.200	90	.017	158	.235	--	---	179	.309	88	.013

^a Taken from 42.9% g_n film as typical 100% g_n bubble.

^b Taken from 22.9% g_n film as typical 100% g_n bubble.

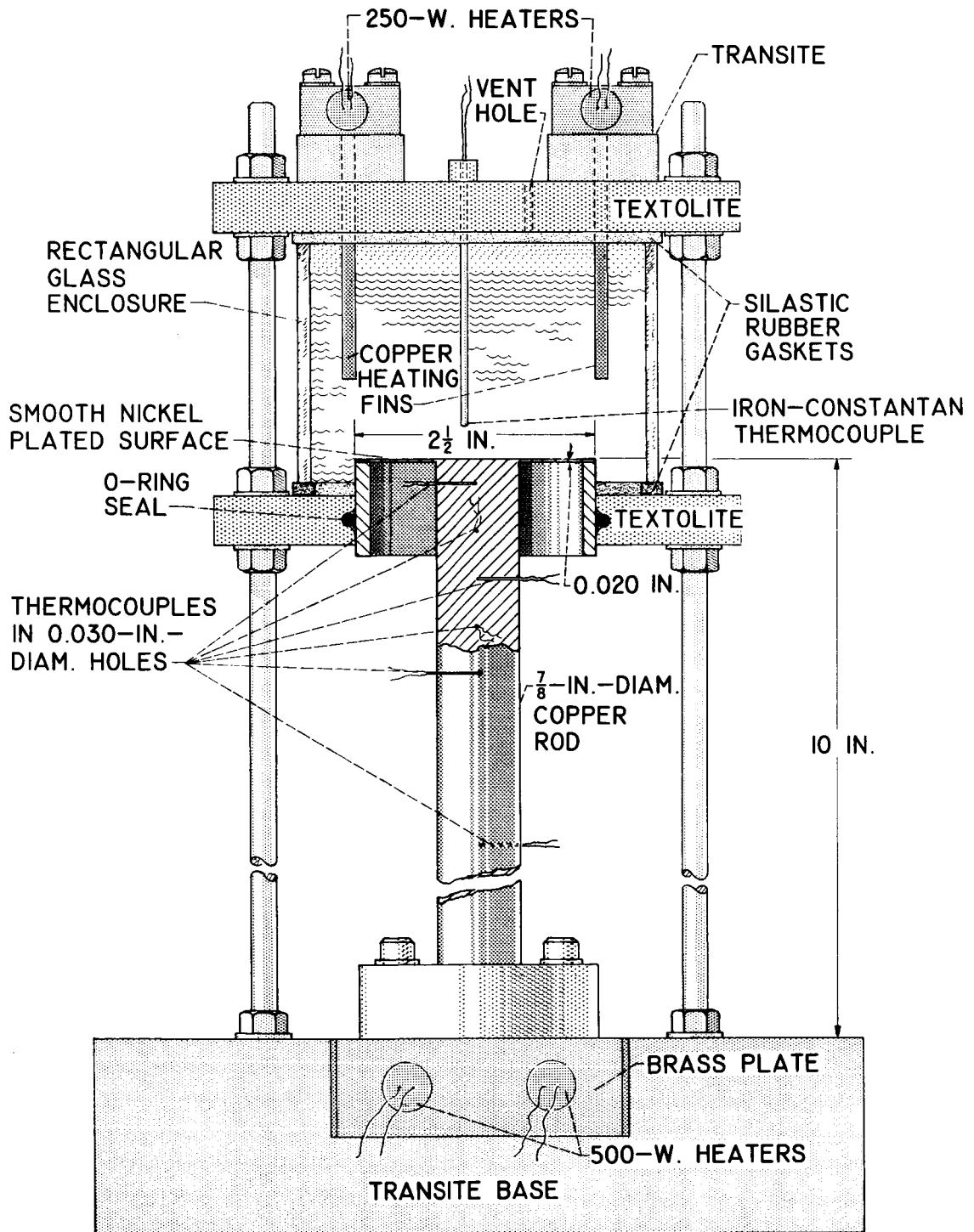
TABLE IV. - VELOCITIES OF FREELY RISING BUBBLES

g/g_n	u_∞ (each number is for a different bubble), in./sec.	Average u_∞ , in./sec.
1	11.34; 11.91; 11.96; 11.85; 11.62; 12.11	11.80
.429	9.69; 9.88	9.79
.229	8.14; 8.57	8.35
.126	6.92; 6.39	6.66
.061	5.83; 5.67	5.75
.030	4.99	4.99
.014	2.5	2.5



(a) Counterweighted drop tower. (Total height, 22.5 ft.).

Fig. 1. - Experimental apparatus.

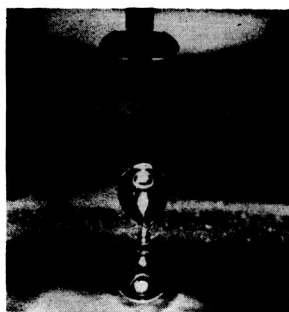


(b) Test boiler assembly.

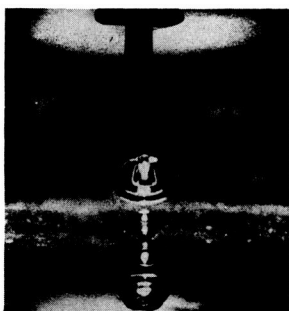
Fig. 1. - Concluded. Experimental apparatus.

CD-7591
-4-5

NORMAL GRAVITY,

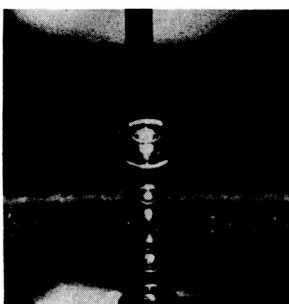
 $1 g_n$ 

0.0007 SEC

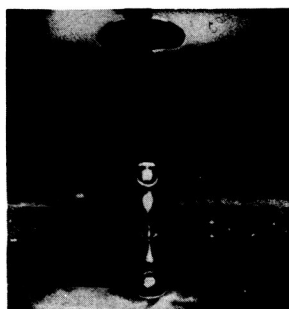


0.006 SEC

→ | ← 1/16"



0.016 SEC

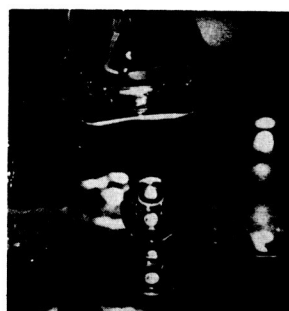


0.045 SEC

REDUCED GRAVITY,

 $0.061 g_n$ 

0.010 SEC



0.030 SEC



0.070 SEC

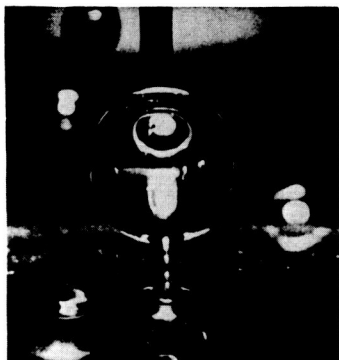
→ | ← 1/16"



0.230 SEC

Fig. 2(a). - Comparison of bubbles growing in normal gravity and 6.1% of normal gravity for site 2. Time is measured from onset of growth for each bubble. (The black vertical probe at the top of each picture is 1/16 in. wide.)

→ | ← 1/16"



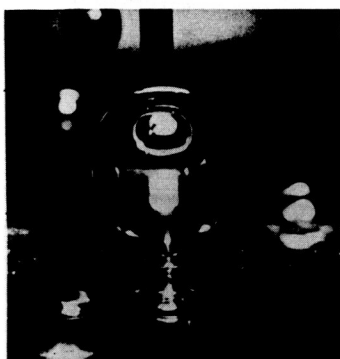
0.236 SEC
FIRST BUBBLE JOINS
DETACHED BUBBLE



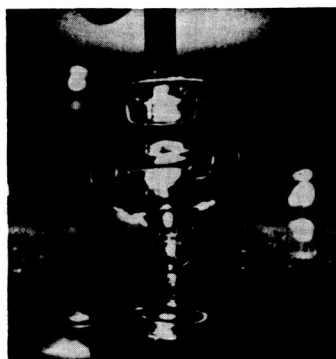
0.250 SEC
SECOND BUBBLE IS
PULLED IN



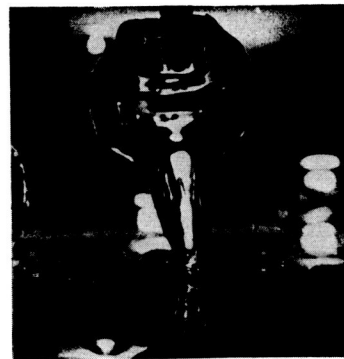
0.303 SEC
FOURTH BUBBLE JOINS
DETACHED BUBBLE



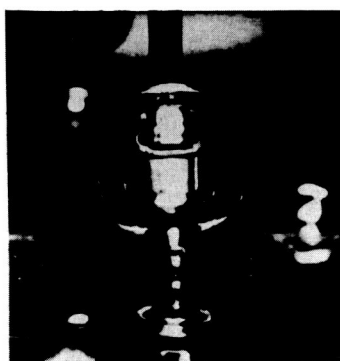
0.2375 SEC
FIRST BUBBLE IS PULLED
INTO DETACHED BUBBLE



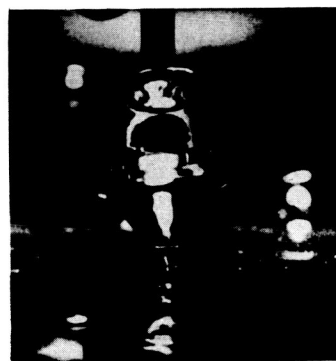
0.265 SEC
THIRD BUBBLE JOINS
DETACHED BUBBLE



0.309 SEC
FOURTH BUBBLE
IS PULLED IN



0.247 SEC
SECOND BUBBLE JOINS
DETACHED BUBBLE



0.268 SEC
THIRD BUBBLE
IS PULLED IN



0.311 SEC
BUBBLE MOVES AWAY AND
NEXT BUBBLE WILL
GROW UNDISTURBED

C-63756

Fig. 2(b). - This is a continuation of the growth of reduced gravity ($0.061 g_0$) bubble in Fig. 2(a). It shows the merging of successive bubbles with undisturbed bubble in Fig. 2(a).

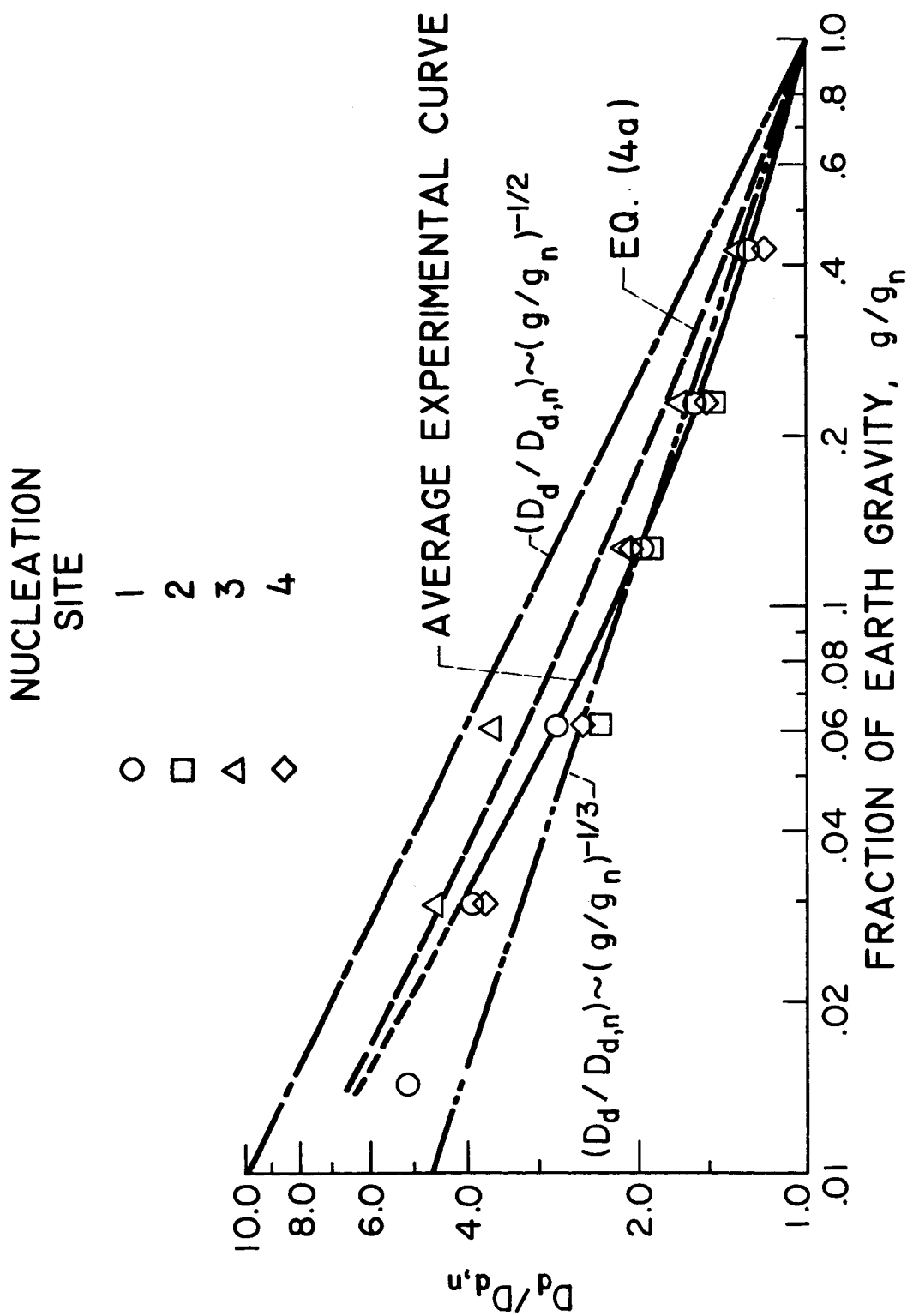
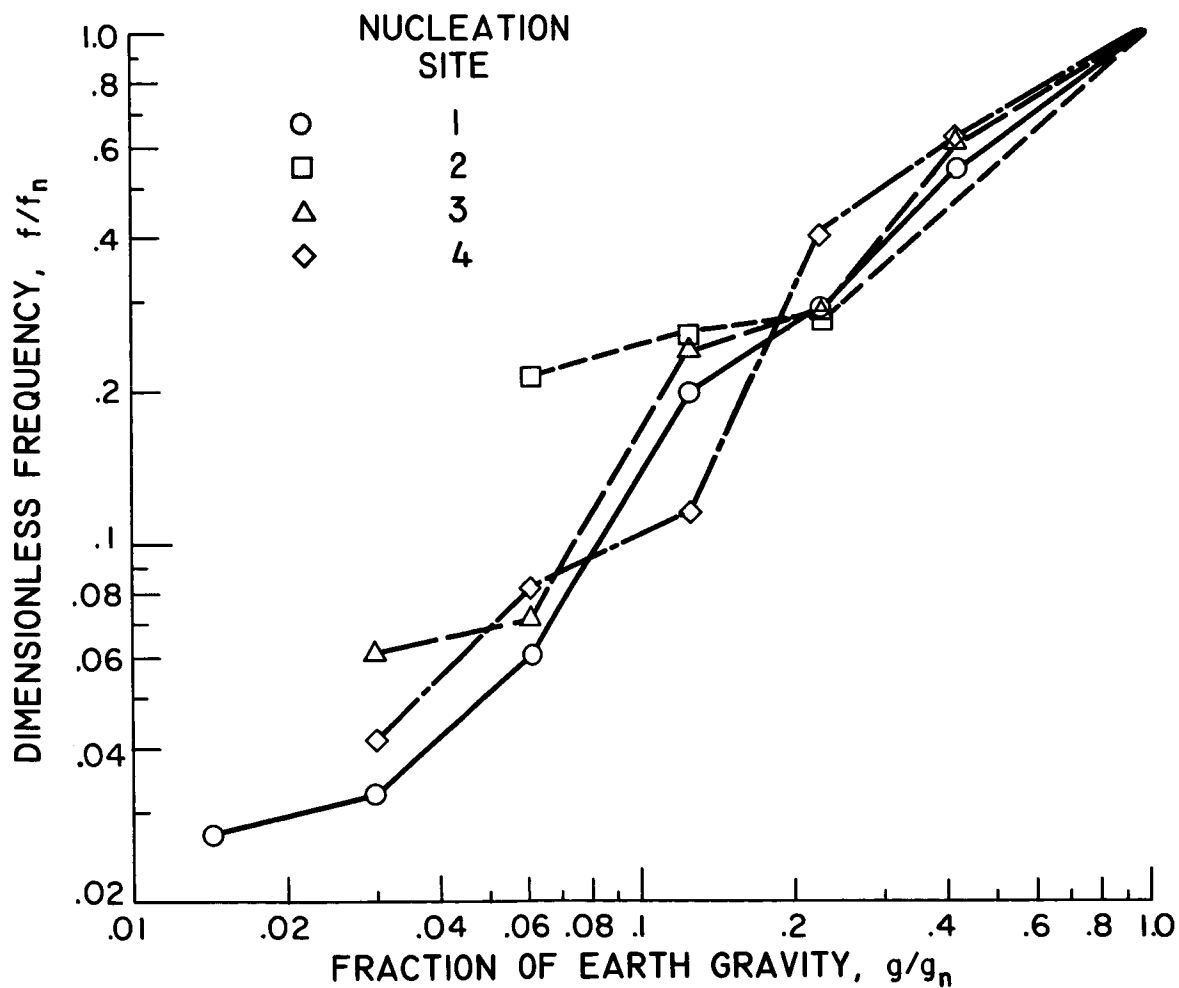
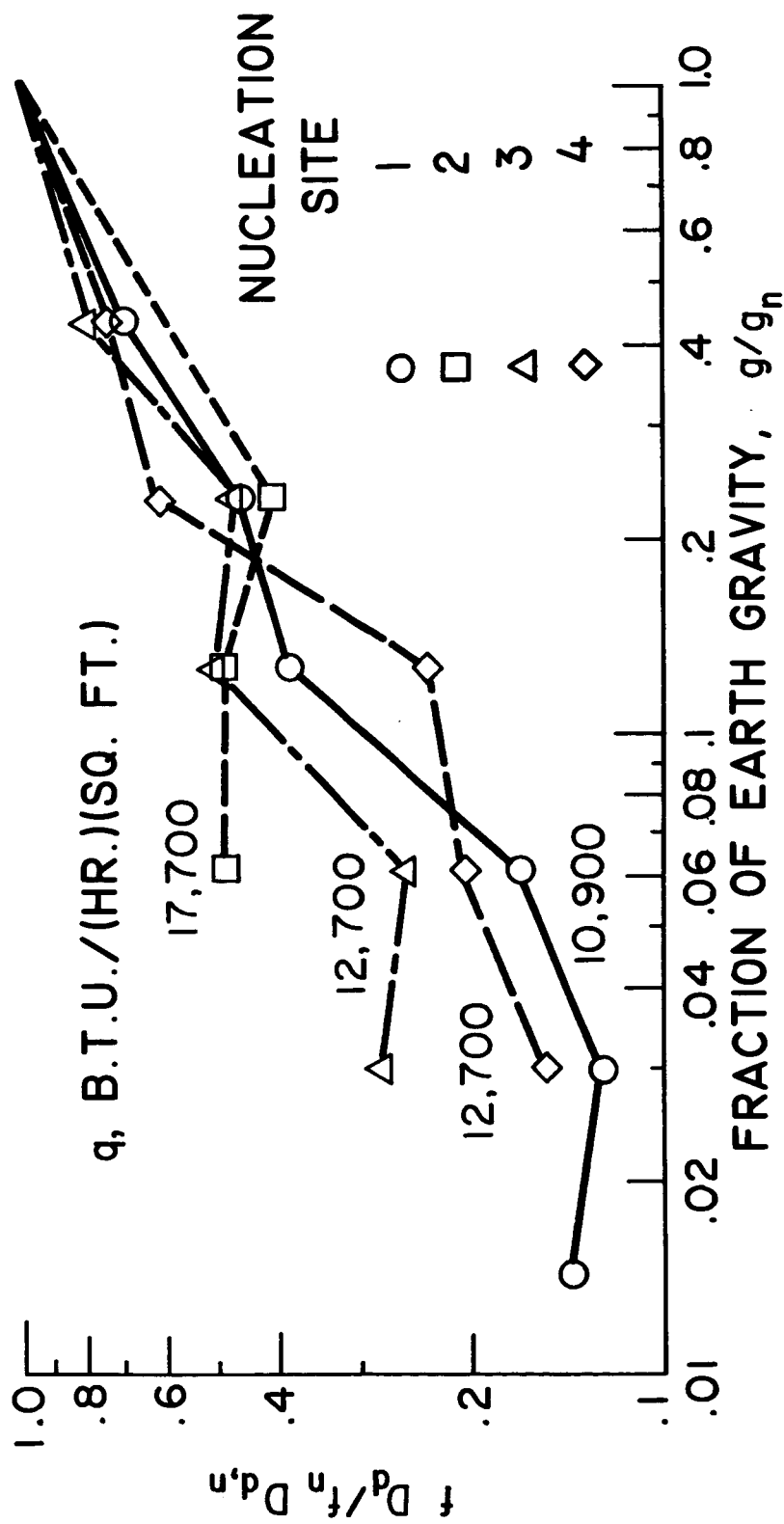


Fig. 3. - Effect of reduced gravity on diameters of single undisturbed bubbles at instant of detachment from surface.



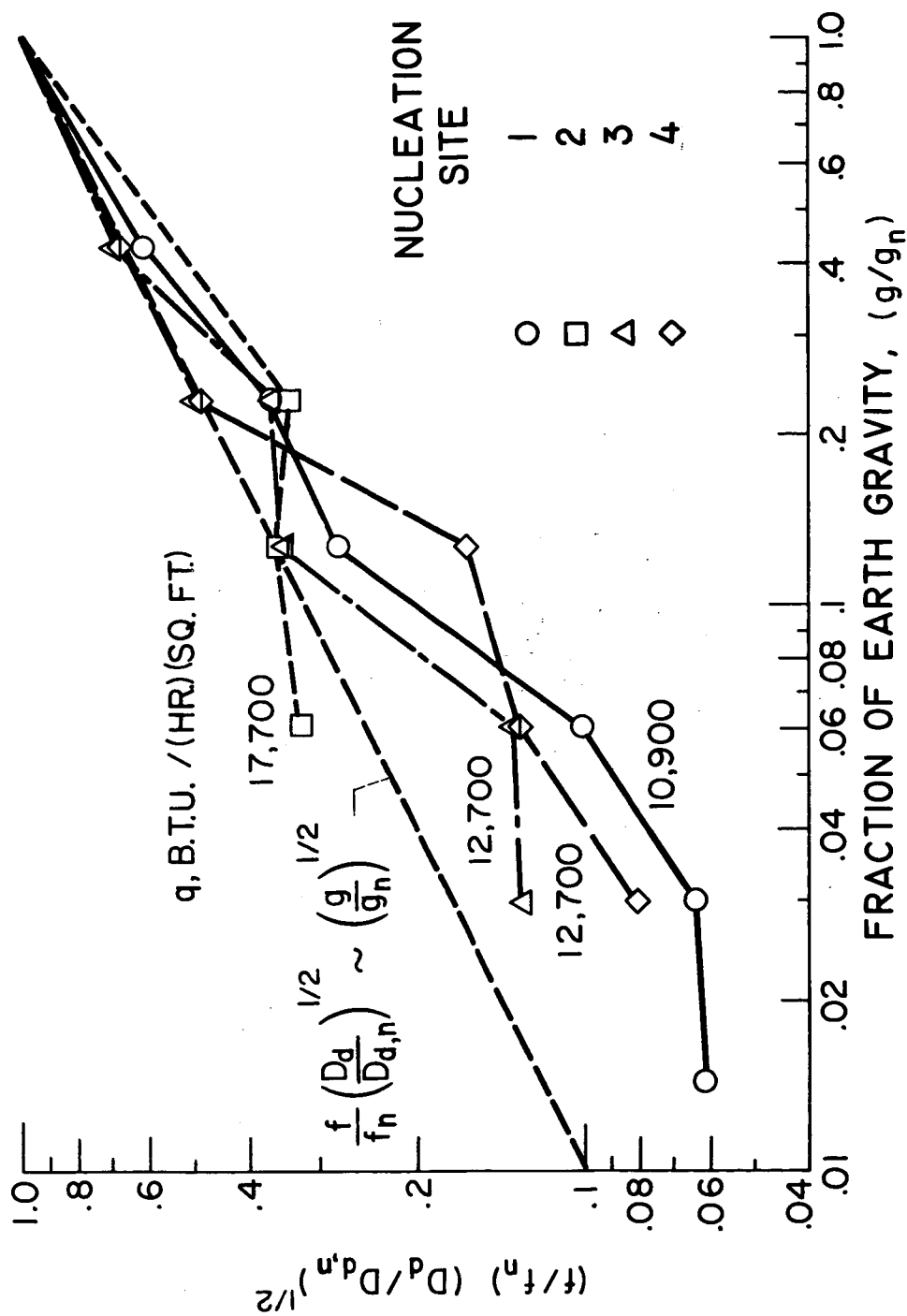
(a) Effect of reduced gravity on frequency (1/growth time) of single undisturbed bubbles.

Fig. 4. - Correlations of frequency and diameter data.



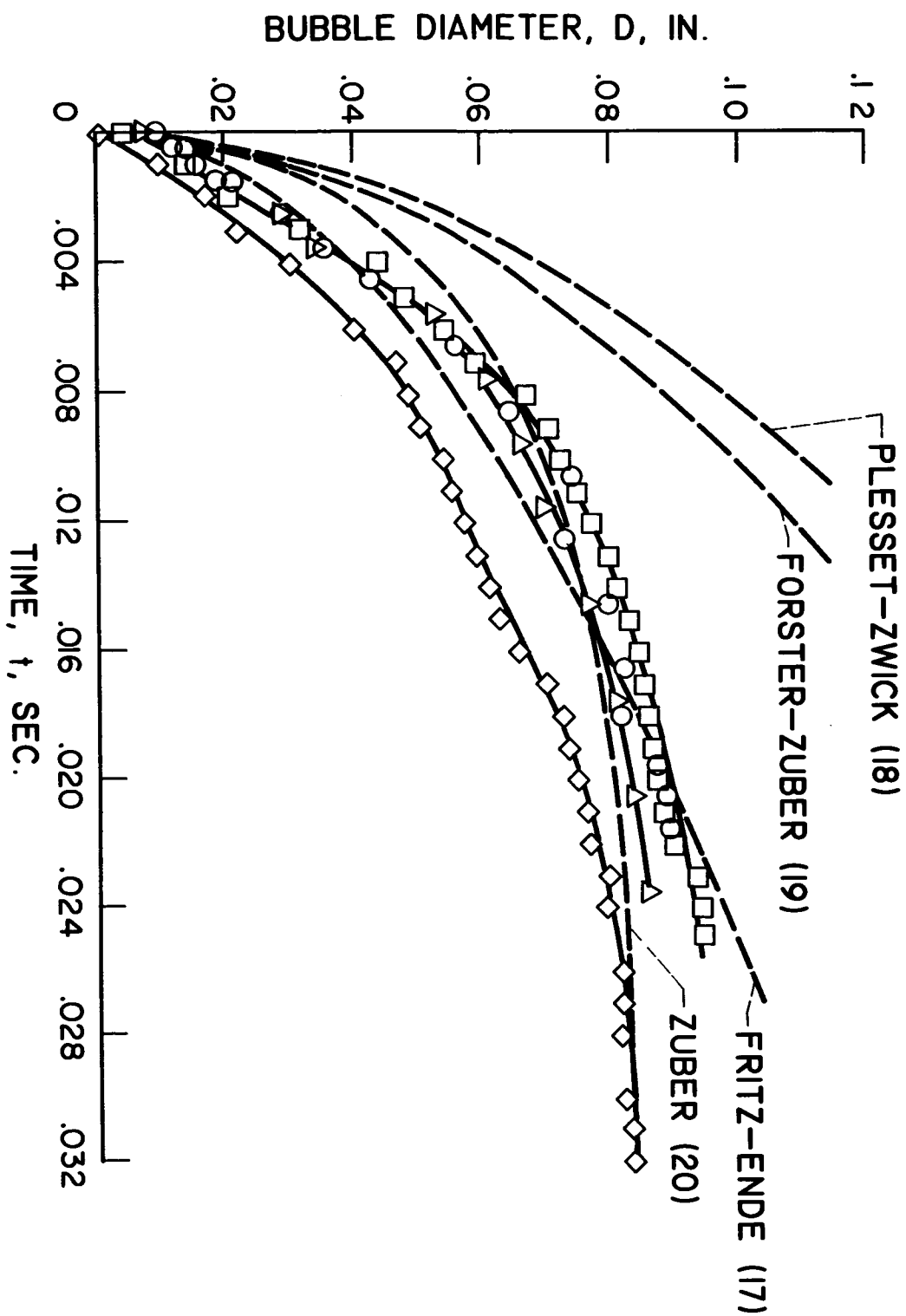
(b) Effect of reduced gravity on frequency-diameter product for single undisturbed bubbles.

Fig. 4. - Continued. Correlations of frequency and diameter data.



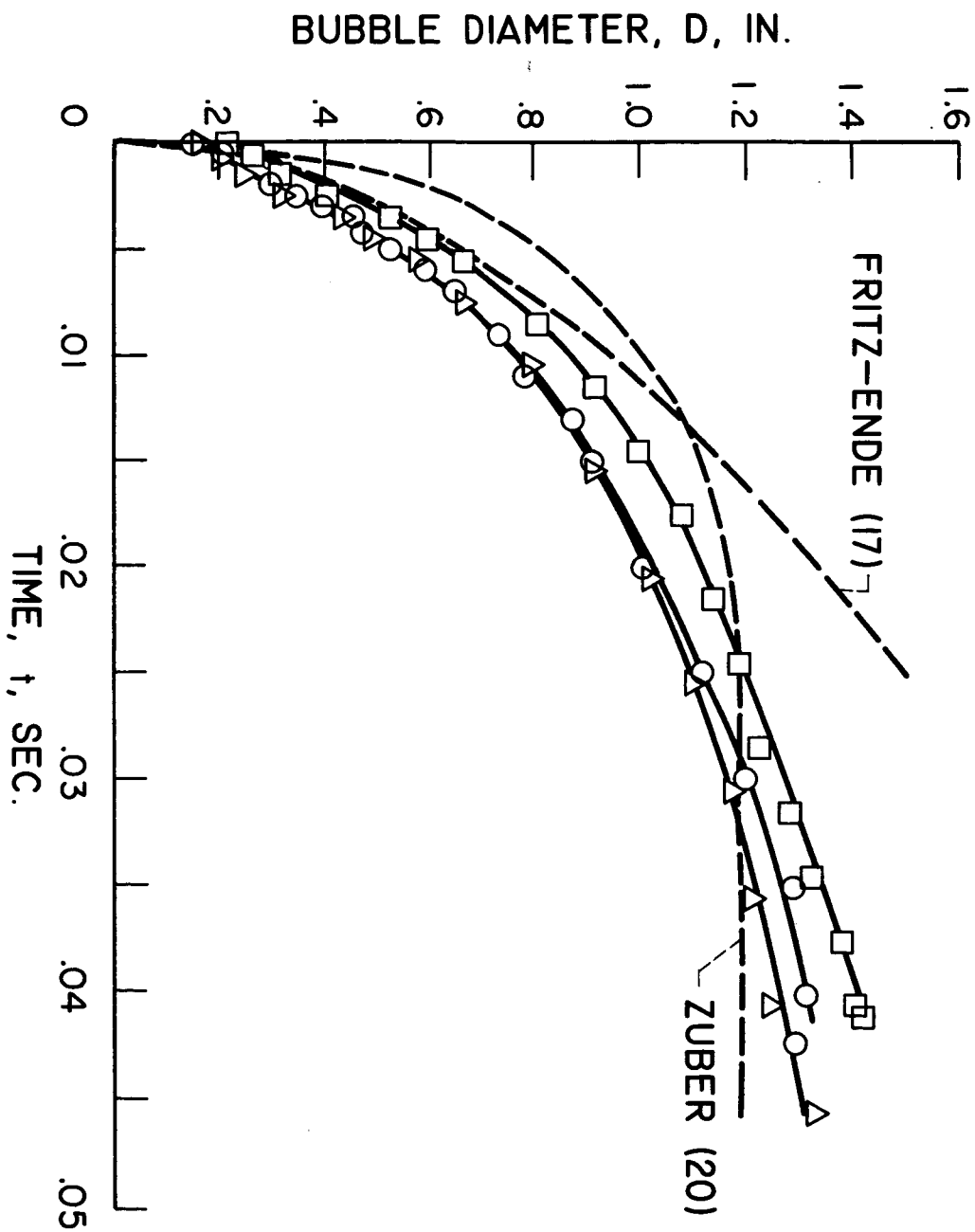
(c) Comparison of frequency-diameter data for single undisturbed bubbles with correlation $fD_d^{1/2} \sim g^{1/2}$.

Fig. 4. - Concluded. Correlations of frequency and diameter data.

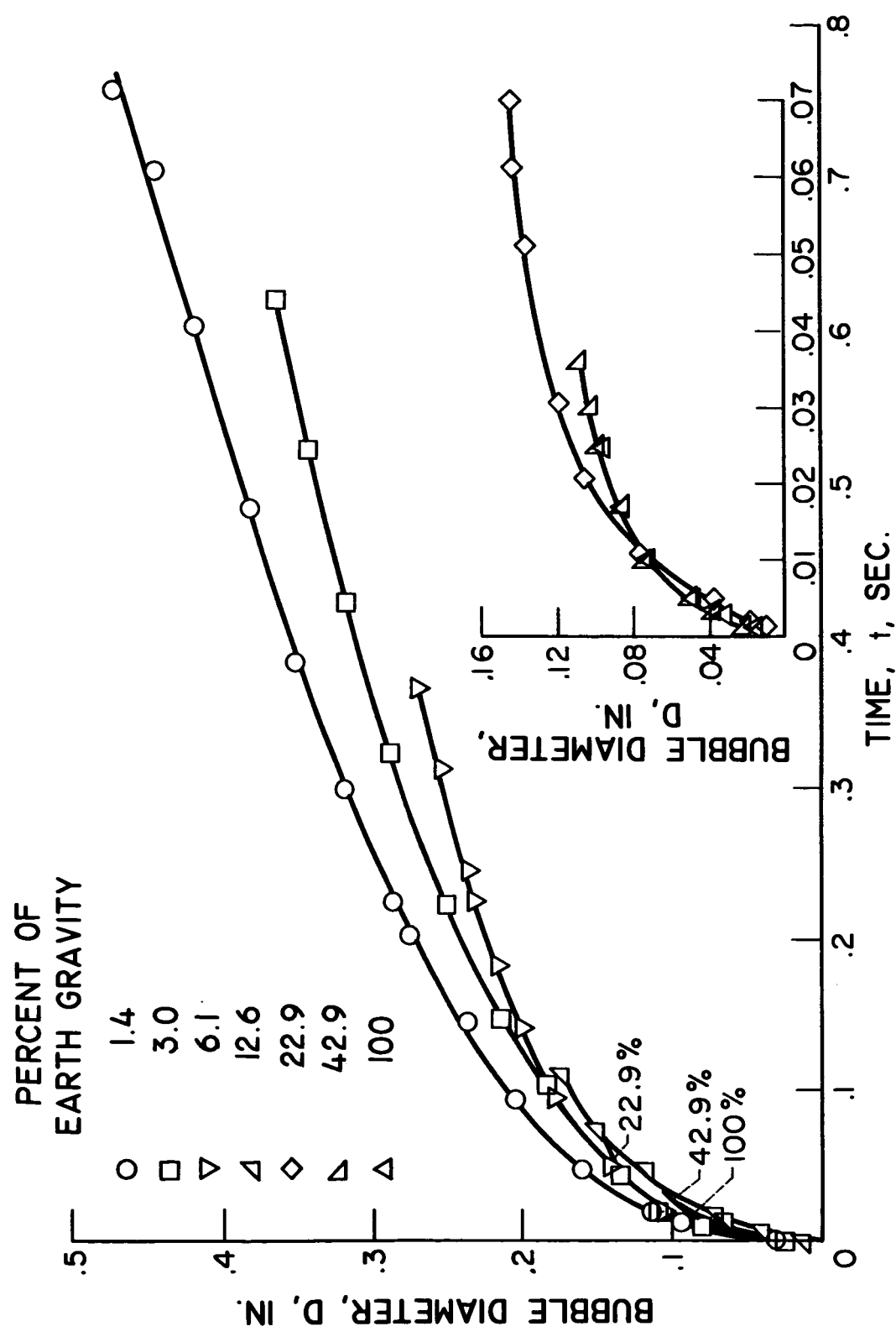


(a) For four typical bubbles in earth gravity; site 1.

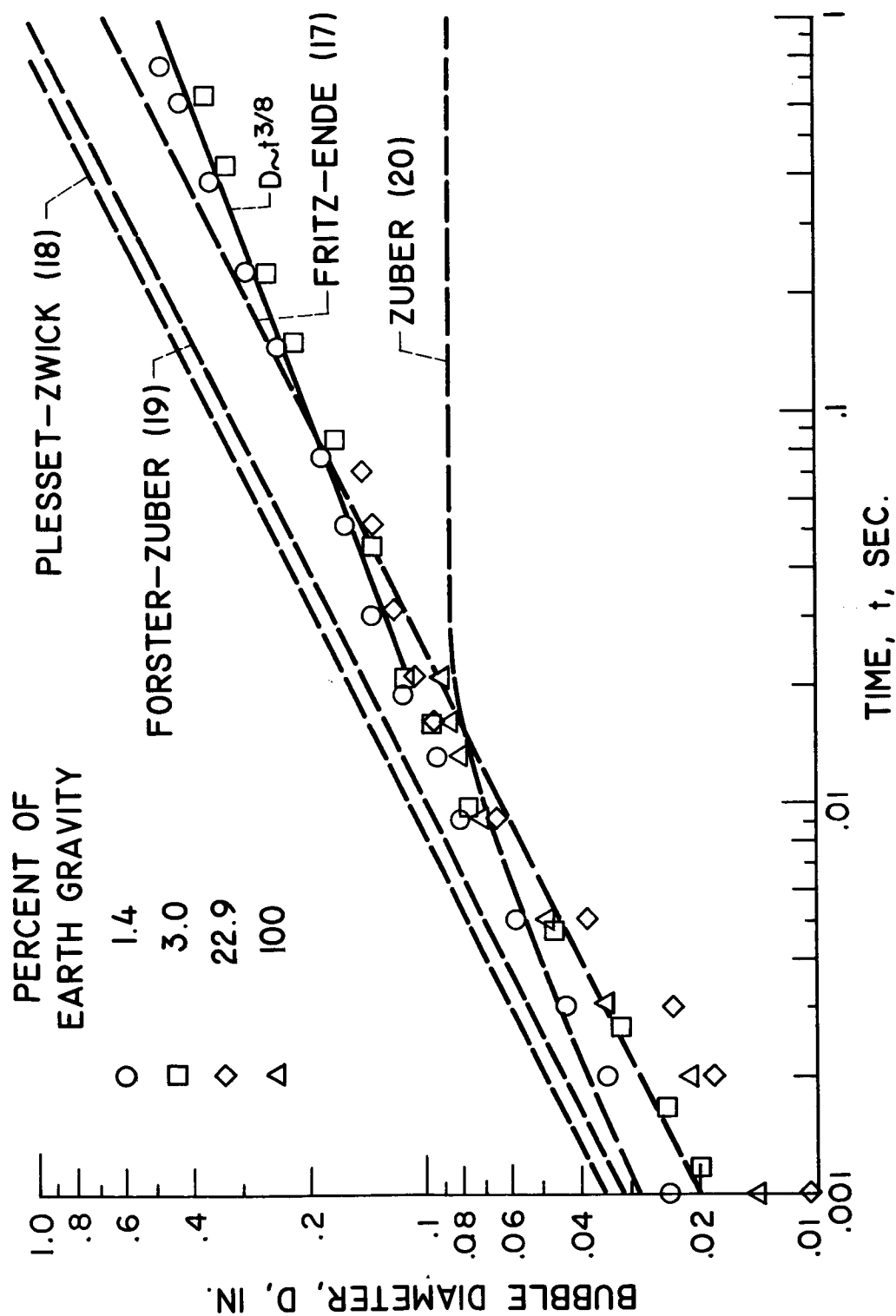
Fig. 5. - Bubble growth data.



(b) For three typical bubbles in earth gravity; site 2.
Fig. 5. - Continued. Bubble growth data.



(c) For typical bubbles in seven different gravity fields; site 1.
Fig. 5. - Continued. Bubble growth data.



(d) For various gravity fields; site 1.

Fig. 5. - Concluded. Bubble growth data.

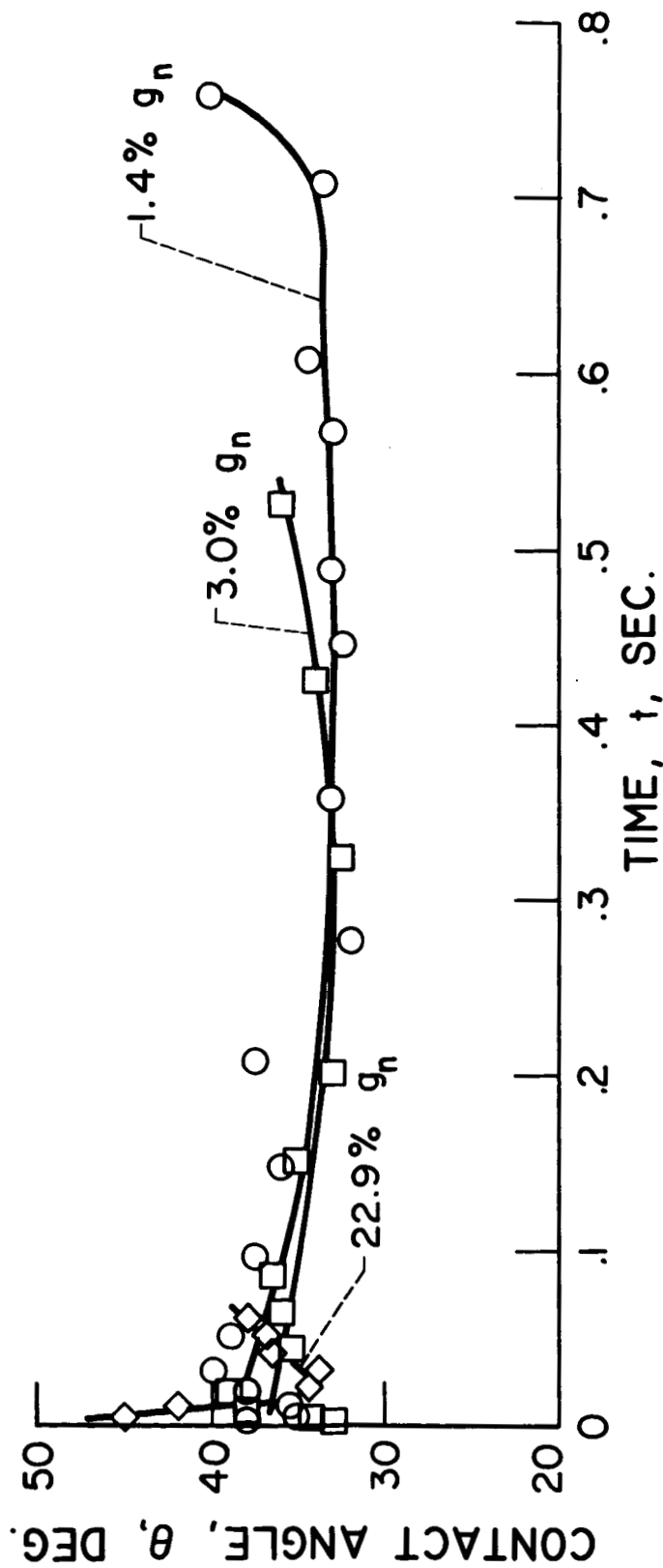


Fig. 6. - Contact angle variation during bubble growth at site 1 for three different gravity fields.

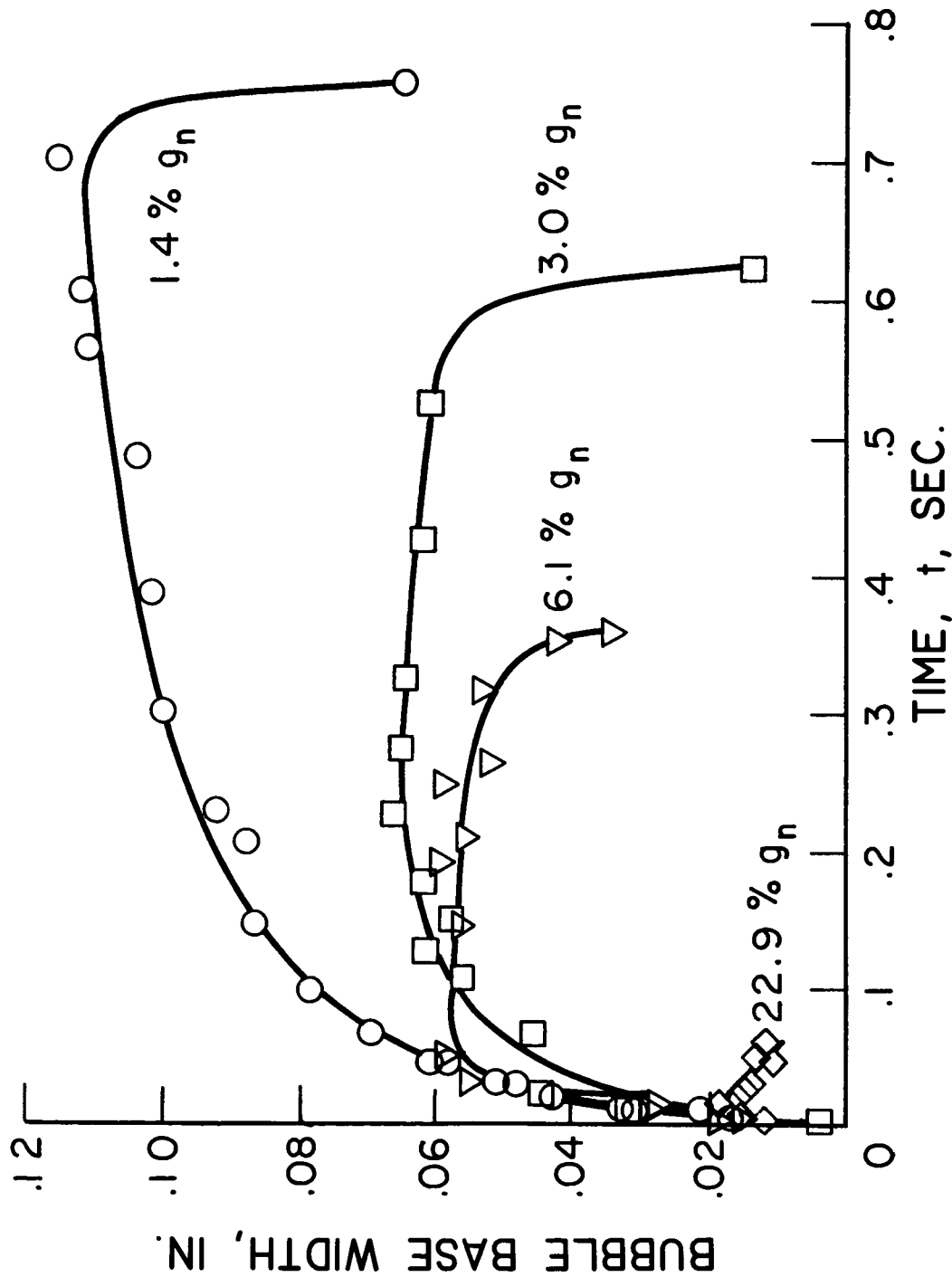
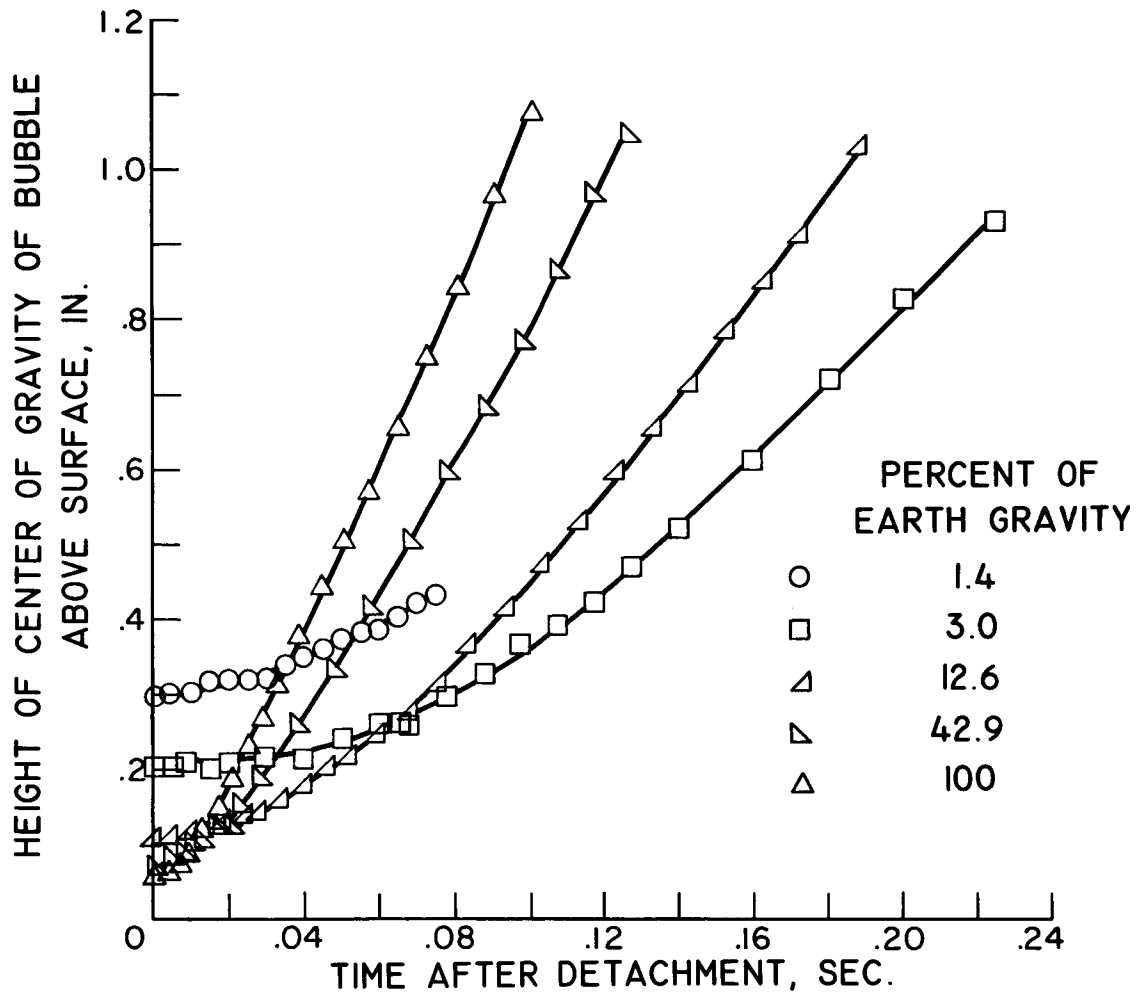
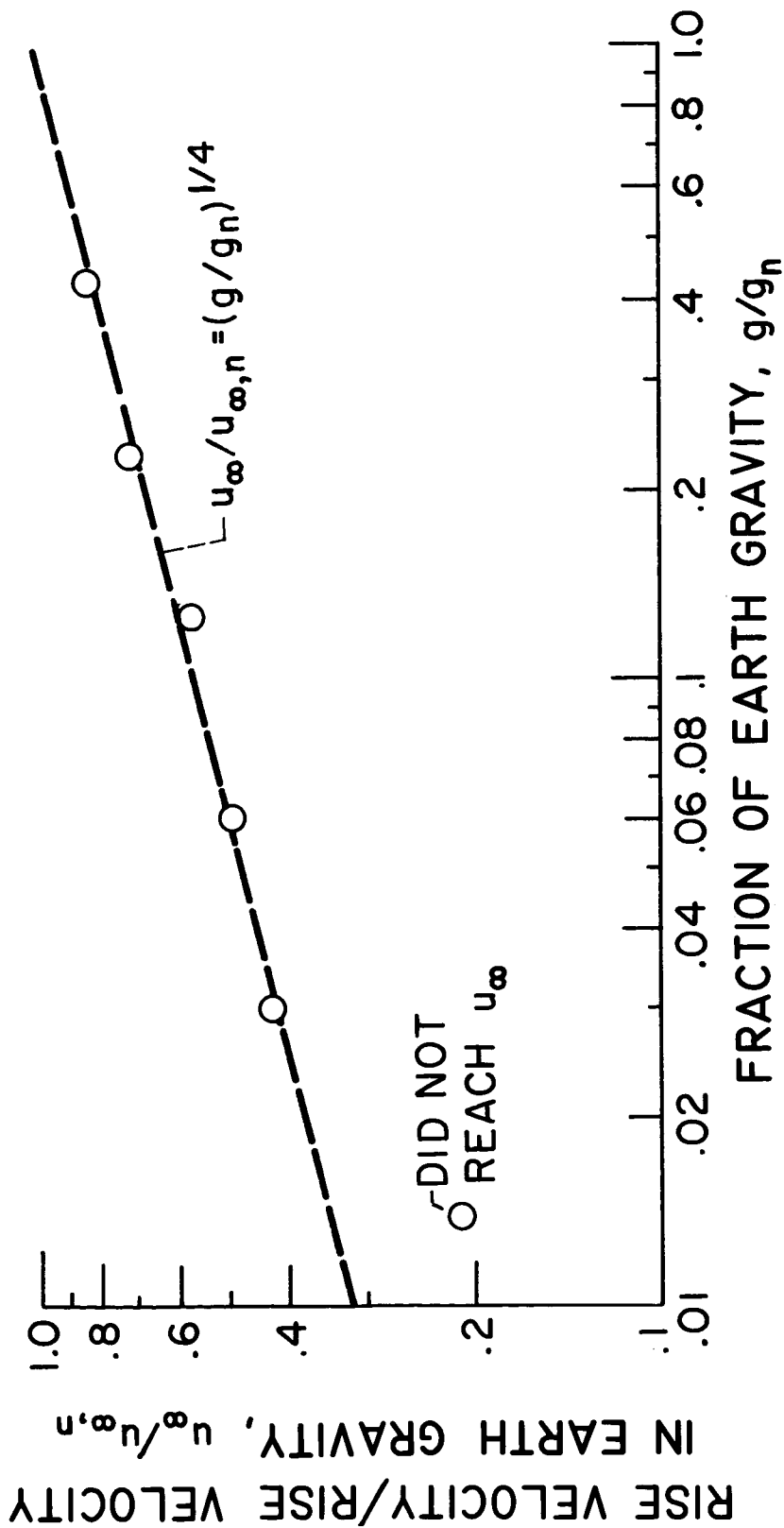


Fig. 7. - Bubble base width (contact circle diameter) variation during growth at site 1 for four different gravity fields.



(a) Rise of center of gravity of bubbles above surface after detachment for five gravity fields; site 1.

Fig. 8. - Behavior of bubbles after detachment.



(b) Effect of gravity field on velocity of freely rising bubbles.
For earth gravity, $u_{\infty,n} = 11.8$ in./sec.

Fig. 8. - Concluded. Behavior of bubbles after detachment.